E&G Quaternary Sci. J., 74, 281–299, 2025 https://doi.org/10.5194/egqsj-74-281-2025 © Author(s) 2025. This work is distributed under the Creative Commons Attribution 4.0 License.





# Transport of heavy minerals and heavy anthropogenic particles in the Rio Sella catchment and along the adjacent coast, northern Spain

Andreas Gärtner<sup>1,2</sup> and Anja Sagawe<sup>3</sup>

<sup>1</sup>Sektion Mineralogie/Isotope Forensics, Museum für Mineralogie und Geologie, Senckenberg Naturhistorische Sammlungen Dresden, Königsbrücker Landstraße 159, 01109 Dresden, Germany

<sup>2</sup>Lehrstuhl für Physische Geographie, Institut für Geographie, Technische Universität Dresden,

Helmholtzstraße 10, 01069 Dresden, Germany

<sup>3</sup>Sektion Paläozoologie, Museum für Mineralogie und Geologie, Senckenberg Naturhistorische Sammlungen Dresden, Königsbrücker Landstraße 159, 01109 Dresden, Germany

**Correspondence:** Andreas Gärtner (andreas.gaertner@senckenberg.de)

Received: 21 May 2025 – Revised: 7 September 2025 – Accepted: 3 October 2025 –

Published: 19 November 2025

**How to cite:** Gärtner, A. and Sagawe, A.: Transport of heavy minerals and heavy anthropogenic particles in the Rio

Sella catchment and along the adjacent coast, northern Spain, E&G Quaternary Sci. J., 74, 281-299,

https://doi.org/10.5194/egqsj-74-281-2025, 2025.

**Abstract:** The Rio Sella in northern Spain drains a catchment area of around 1200 km<sup>2</sup>. It originates in the Picos

de Europa and erodes a variety of outcropping lithologies, mainly of Palaeozoic and minor Mesozoic to Cenozoic age. These rocks include siliciclastics, their metamorphic equivalents, carbonates and mixed sedimentary lithologies but almost no (meta-)igneous rocks. Some of the mentioned rock types are only found in specific areas within the study area, and most of them are identified by specific heavy mineral associations. It is therefore possible to make preliminary estimates of the potential detrital heavy mineral contribution of each region in the Rio Sella catchment. Further sampling of modern, i.e. currently deposited, river and beach sediments allows for sediment routing during transport and recycling processes. This also includes the impact of grain size effects and signal dilution due to different heavy mineral fertilities of the eroded strata. The influence of anthropogenic activities is reflected by the abundance of heavy anthropogenic particles, and the potential of this for sediment research or environmental impact is yet to be determined. The initial results indicate the potential and necessity of detailed heavy mineral characterisation of both fluvial sediments and outcropping lithologies within a catchment. This is particularly important when aiming to reconstruct sedimentary

and particle fluxes at a high spatial resolution.

Kurzfassung: Der Rio Sella im Norden Spaniens entwässert ein Einzugsgebiet von rund 1200 km<sup>2</sup>. Er entspringt

in den Picos de Europa und erodiert eine Vielzahl von aufgeschlossenen, hauptsächlich paläozoischen sowie in geringerem Maße meso- und känozoischen Lithologien. Zu diesen Gesteinen gehören Siliziklastika, ihre metamorphen Entsprechungen, Karbonate und gemischte sedimentäre Lithologien, jedoch fast keine (meta-) magmatischen Gesteine. Einige der genannten Gesteinsarten kommen nur in bestimmten Bereichen des Untersuchungsgebiets vor. Die meisten von ihnen lassen sich anhand

spezifischer Schwermineralassoziationen identifizieren. Daher ist es möglich, vorläufige Schätzungen zum potenziellen Beitrag der detritischen Schwerminerale jeder Region im Einzugsgebiet des Rio Sella vorzunehmen. Weitere Probenahmen von modernen, d.h. derzeit abgelagerten Fluss- und Strandsedimenten ermöglichen eine Verfolgung der Sedimente während des Transports und der Recyclingprozesse. Dazu gehören auch die Auswirkungen der Korngröße und die Signalverdünnung aufgrund unterschiedlicher Schwermineralgehalte der erodierten Schichten. Der Einfluss anthropogener Aktivitäten spiegelt sich in der Häufigkeit schwerer anthropogener Partikel wider, deren Potenzial für die Sedimentologie oder die Umweltverträglichkeit noch zu bestimmen ist.

### 1 Introduction

The steepest ca. 10% of terrestrial mountainous areas may contribute more than 50% of the total denudation (Larsen et al., 2014). In particular in such settings, rivers transport most of the eroded material to the oceans (Pitlik et al., 2021), being ideal for detailed studies on fluvial particle transport. Various factors, like lithology, grain size, climate and morphology (Neely and DiBiase, 2023), control the amount of transported sediments in specific mountainous catchments. However, some mechanisms of sediment transport from the headwaters of mountainous rivers to the ocean, including temporal sediment storage, are not known in detail (Misset et al., 2019; Pitlik et al., 2021), nor is the subsequent alongshore transport of their sediments (Milliman and Syvitski, 1992; Syvitski and Milliman, 2007). The comparatively small drainage of the Rio Sella of northern Spain is one such steep river and was therefore chosen for detailed studies on single particle transport.

Traditionally, heavy minerals, i.e. minerals with a density of  $> 2.80\,\mathrm{g\,cm^{-3}}$ , either in large mineral spectra (van Andel, 1950; Yang et al., 2009) or with focus on a specific mineral group (Gärtner et al., 2014; Oberthür et al., 2016), play an important role when reconstructing sediment transport and provenance. To achieve information on sediment transport in the Rio Sella catchment of northern Spain, 37 samples of outcropping sedimentary rock and modern, i.e. currently deposited, sediments were analysed (Fig. 1).

Aside from natural sediment transport, anthropogenic activities may change the mechanisms of sediment transport in rivers (Jing et al., 2022; Korup, 2012) and along shorelines (Stevens et al., 2024). Finally, human activity releases enormous amounts of anthropogenic materials, which go far beyond microplastics and also contain heavy anthropogenic particles (HAPs), like metal spheres, fragments of alloys, heavy glasses (Scholz and Gärtner, 2024) and other materials, whose behaviour in sediments remains unstudied. The accidental finding of these particles led to an initial characterisation of this material within the Rio Sella catchment.

### 2 The Rio Sella catchment

Located in the eastern Asturias and northernmost Castilla y Léon provinces, the perennial Rio Sella has a catchment area of ca. 1284 km<sup>2</sup>, while its source is at about 1100 m a.s.l. in the region of the Picos de Europa. Having a main channel length of about 66 km, the resulting mean gradient is ca. 20 %o. The main tributaries of the Rio Sella are the Rios Piloña, Ponga, Dobra and Güeña.

### 2.1 Quaternary terrace levels and inferred maximum incision rates

Along the river, up to 12 terrace levels are developed (Ruiz Fernández and Poblete Piedrabuena, 2011), of which the 8 m terrace has an apparent minimum age of 11.3 to 14.3 ka (Fernández Irigoyen et al., 2006). The highest terrace level at 110 m above the river is known for Acheulean tool finds (Fernández Irigoyen et al., 2006), which results in a likely minimum age of ca. 130 ka (Key et al., 2021) for these deposits. Thus, maximum incision rates are around 0.8 to 0.6 mm a<sup>-1</sup>, which is in line with findings from adjacent catchments (Ruiz Fernández and Poblete Piedrabuena, 2011). Furthermore, larger landslides have been dated at ca. 2.65 ka based on <sup>14</sup>C (Fernández Irigoyen and Ruiz Fernández, 2008).

### 2.2 Geology of pre-Quaternary rocks

The Rio Sella catchment is covered by eight sheets of the 1:50 000 geological map of Spain (Alvarez-Marrón et al., 1990; Caride et al., 1975; Gervilla et al., 1973a, b; Hereida and Rodríguez Fernández, 1989; Hereida et al., 1990; Julivert and Navarro, 1984; Navarro and Leyva, 1986). While Early Permian igneous rocks of rhyolitic, granodioritic and gabbrodioritic composition of the Infiesto Plutonic Complex (López-Gómez et al., 2019; Suárez et al., 1993) to the west are limited to only ca. 0.1% of the investigated area, the general lithology of the Rio Sella catchment comprises a wide range of siliciclastic (ca. 26.7 area %), carbonate (ca. 46.7 area %) and mixed siliciclastic and carbonate (ca. 24.7 area %) sedimentary rocks (e.g. Gervilla et al., 1973c). The remaining ca. 2.0 % of the catchment are covered by scree and landslides made from various lithologies (Fig. 2). Therefore, siliciclastic and carbonate rock occurrences are almost

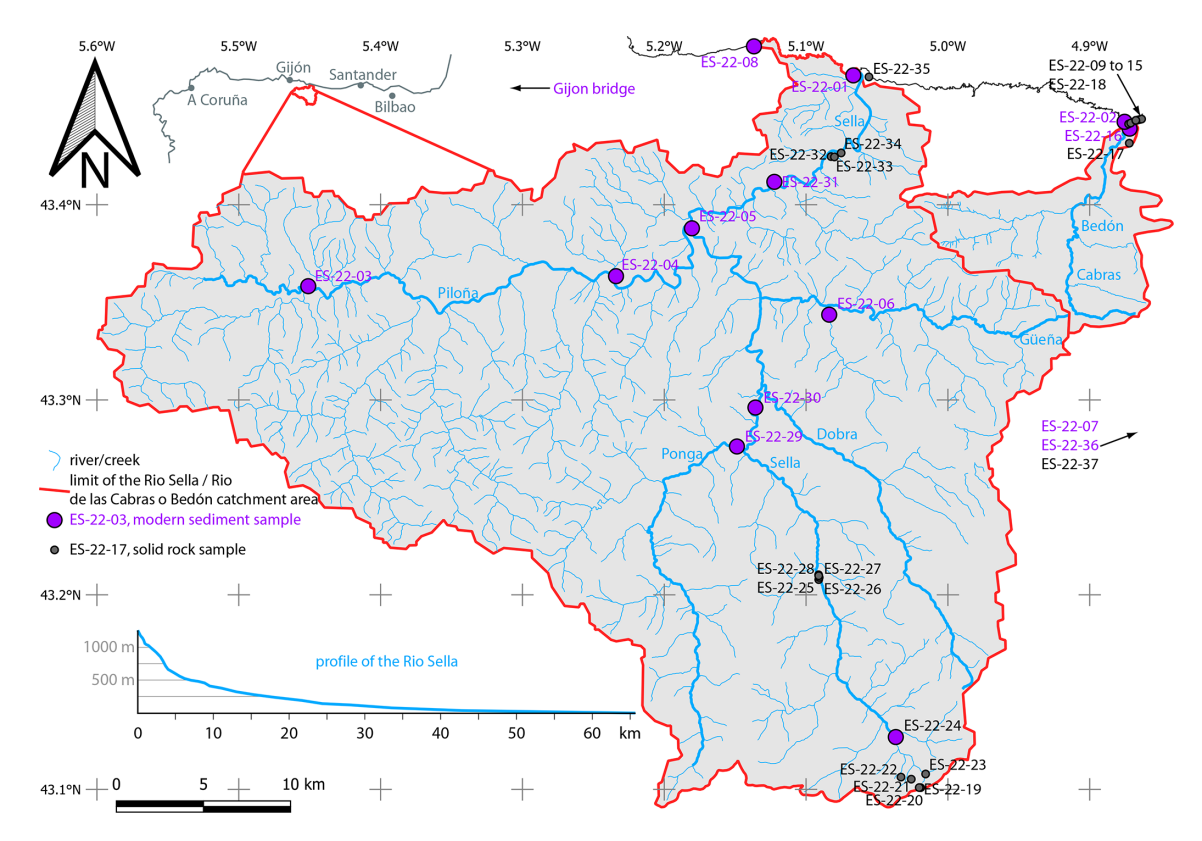


Figure 1. The drainage system of the river Sella and the sampling localities of this study. The inset illustrates the hypsometric profile of the river.

equally covering the study area, while the occurrence of igneous rocks is negligible.

With regard to the objective of the study, the description of geological units and stratigraphy is succinctly outlined in the following paragraphs. The oldest rocks in the Rio Sella catchment are represented by the dolostones, limestones and occasional shales of the Early Cambrian Lancara Formation (Perejón et al., 2012; Zamarreño and Julivert, 1967). These are overlain by mainly siliciclastic Mid- to Late Cambrian Oville and Ordovician Barrios formations (Aramburu and García-Ramos, 1993; Gutiérrez-Alonso et al., 2007; Palacios, 2015). Discordantly overlying Devonian-aged (Famennian) rocks are limited to the comparatively thin outcrops of the siliciclastic Ermita Formation (Colmenero, 1976; Sanz-López and Blanco-Ferrera, 2023; van Loevezijn and Raven, 2021).

Large parts of the Rio Sella catchment are covered by Carboniferous carbonate rocks but also shale and other pelitic to psammitic siliciclastics (Fig. 3). Several formations are distinguished in certain areas of the catchment area, starting with the black shales of the Tournaisian Vegamián Formation (Borrego et al., 2018). Up-section follows the Visean–Serpukhovian Alba and the Serpukhovian–Bashkirian Barcaliente formations (Blanco-Ferrera et al., 2021). When dealing with post-Serpukhovian Carboniferous strata, the area is separated into the western Ponga Nappe Unit, the southern

Pisuerga—Carrion Unit and the eastern Picos de Europa Unit, with each of them containing differently termed formations spanning to the Moscovian (for details, see Bahamonde et al., 1997; Blanco-Ferrera et al., 2021). Kasimovian and Ghzelian (Late Carboniferous) strata are represented by the rocks of the Pando and Maraña-Brañas groups (Motis et al., 2001).

Permian strata including carbonate and siliciclastic rocks discordantly overlie the Carboniferous series in the western parts of the catchment area (Sotres and Cabranes formations; Weil et al., 2010), while an isolated occurrence of undefined Permo–Triassic age is located to the east.

The earliest Mesozoic rocks in the catchment are represented by Triassic siliciclastic strata (Lugas Unit), overlain by evaporite rocks (Fuentes Unit; Suárez Rodriguez, 1988). Triassic rocks are limited to the western and northwestern margins of the Rio Sella catchment.

Early (Hettangian) to Late Jurassic (Kimmeridgian-Tithonian) rocks are mainly located in the northern parts of the Rio Sella catchment. They form a sequence of about 600 m thickness. These rocks are subdivided from base to top into the Gijón, Rodiles, Vega, Tereñes and Lastres formations. The Jurassic strata represent intercalations of dolostone, limestone, marl, red shale, conglomerate and sandstone (Avanzini et al., 2007; Navarro and Leyva, 1986; Valenzuela Fernández, 1989).

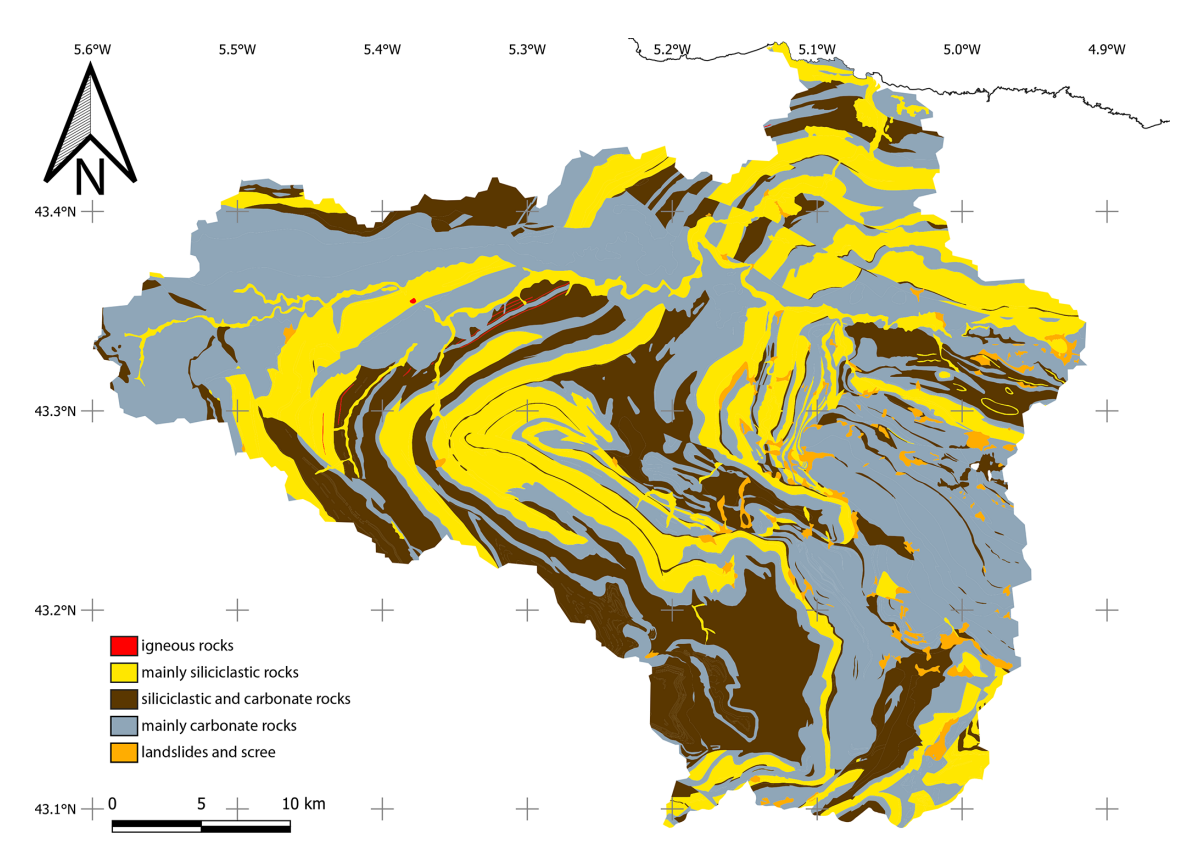


Figure 2. Lithological overview of the Rio Sella catchment (derived from Alvarez-Marrón et al., 1990; Caride et al., 1975; Gervilla et al., 1973a, b; Hereida and Rodríguez Fernández, 1989; Hereida et al., 1990; Julivert and Navarro, 1984; Navarro and Leyva, 1986).

A narrow band of Cretaceous, Barremian to Santonian (Gervilla et al., 1973c, Hereida and Rodríguez Fernández, 1989), consisting of minor siliciclastic and mainly carbonate sedimentary rocks, stretches out from east to west through the entire catchment area and rests unconformably above the older rocks (Fig. 3; González-Fernández et al., 2014).

Finally, parts of the Cretaceous deposits are covered by Palaeocene to Oligocene (Gervilla et al., 1973a, b) to possibly Neogene carbonate rocks.

### 2.3 Anthropogenic influences

Anthropogenic influences in the Rio Sella catchment are concentrated along the middle and lower reaches of larger rivers and the coast. This is particularly mirrored by the distribution and density of highways, roads and paths and railways, and the population density (Fig. 4). Aside from the coast and archaeological sites, the Picos de Europa National Park attracts around 2 million additional tourists per year, of which up to 1 million visit the lakes of Cavadonga (López and Pardo, 2018), which are mainly reached via the Sella valley. The ascending trend of visitors was only shortly interrupted by COVID-19 during 2019 to 2021 (Molteni, 2022). Therefore, even the least-inhabited regions of the Rio Sella catchment

are disproportionately highly frequented by persons and traffic.

### 3 Material and methods

Twenty-two samples were taken from the main outcropping lithologies that occur in the Rio Sella catchment ("pre-Quaternary rocks"), while eight stream sediment samples are used to characterise the modern river heavy-mineral signal of the Rio Sella. A further sample was taken from the lower reaches of the adjacent ca. 23 km long Rio de las Cabras o Bedón. Six additional samples of beach sediment between Gijón and Cóbreces were analysed (Table 1). These beach sediments were collected close to the current swash zone, with obvious heavy mineral bands and placers being avoided.

For heavy mineral analyses at the Senckenberg Naturhistorische Sammlungen Dresden, approximately 10 to 20 g of each sample was used for the heavy mineral separation procedure. Each hard rock sample was crushed by hand, as this is less destructive than using a mill or jaw crusher. While some broken grains were inevitable, microscopic and scanning electron microscope images suggest that many grains remained unaffected. All samples were sieved for the fraction  $< 630\,\mu m$  and weighed (Sartorius Secura 224 – 1S, accuracy = 0.1 mg, reproducibility = 0.1 mg,

Table 1. Main data of the samples presented in this study. For further information, see Table S1 in the Supplement.

Sample ID	Location	Rock type	Latitude	Longitude	Stratigraphic age
Beach sample	Beach samples from W to E				
Gijón Bridge	playa Gijón/Rio Piles	beach/fluvial sediment	43.541083	-5.645167	modern/Holocene
ES-22-08	playa de Vega	beach sediment	43.480600	-5.136740	modern/Holocene
ES-22-01	playa Ribadesella	beach sediment	43.465760	-5.066660	modern/Holocene
ES-22-02	playa de St. Antolin	beach sediment	43.442030	-4.875380	modern/Holocene
ES-22-07	playa Celorio	beach sediment	43.431570	-4.808870	modern/Holocene
ES-22-36	playa de Luaña	beach sediment	43.393720	-4.220470	modern/Holocene
Samples of riv	Samples of river sediments from headwaters to mouth				
ES-22-24	Arroyo de Fonsella	fluvial sediment	43.126480	-5.036730	modern/Holocene
ES-22-29	Rio Ponga	fluvial sediment	43.275700	-5.148760	modern/Holocene
ES-22-30	Rio Sella	fluvial sediment	43.295670	-5.135710	modern/Holocene
ES-22-06	Rio Reinazo o Cavadonga	fluvial sediment	43.343270	-5.083690	modern/Holocene
ES-22-03	Rio Peloña	fluvial sediment	43.357880	-5.451060	modern/Holocene
ES-22-04	Rio Peloña	fluvial sediment	43.363000	-5.234030	modern/Holocene
ES-22-05	Rio Sella	fluvial sediment	43.387510	-5.180480	modern/Holocene
ES-22-31	Rio Sella	fluvial sediment	43.411300	-5.122360	modern/Holocene
Samples of riv	Samples of river sediments outside of Rio Sella catchment				
ES-22-16	Rio de las Cabras o Bedón	fluvial sediment	43.438520	-4.871830	modem/Holocene
Basement samples	ples				
ES-22-37	Bielba Fm., Siliciclastic Mbr.	sandstone	43.394490	-4.219570	Cretaceous, Late Albian
ES-22-35	Tereñes y Lastres Fm.	calcareos pelite	43.464970	-5.055660	Jurassic, Late Malm
ES-22-19	Pontón Gp.	shale	43.100450	-5.019210	Carboniferous, Ghzelian to Kasimovian (Early Stefanian)
ES-22-20	Pontón Gp.	shale	43.100490	-5.020210	Carboniferous, Early Kasimovian
ES-22-22	Lechada Fm.	shale	43.105880	-5.033070	Carboniferous, Kasimovian-Bashkirian (Westfalien A-D)
ES-22-17	no Fm. name, No 12 on map	calcareous pelite	43.431077	-4.872061	Carboniferous, Kasimovian (Stefanian)
ES-22-21	Lechada Fm.	conglomerate, matrix	43.104820	-5.025820	Carboniferous, Moscovian
ES-22-25	"Caliza de Montaña"	limestone	43.207390	-5.091070	Carboniferous, Bashkirian-Serpukhovian (Namurian)
ES-22-26	"Caliza de Montaña"	limestone	43.208490	-5.090720	Carboniferous, Bashkirian-Serpukhovian (Namurian)
ES-22-13	Barcaliente Fm.	limestone, white	43.444030	-4.862670	Carboniferous, Bashkirian-Serpukhovian (Namurian)
ES-22-14	Caliza "griotte"/Grioto Fm. and equivalents	limestone, black, "Stinkkalk"	43.443430	-4.863390	Carboniferous, Serpukhovian–Visean (earliest Namurian)
ES-22-11	Caliza "griotte"/Grioto Fm. and equivalents	limestone, red	43.442930	-4.866130	Carboniterous, Visean
ES-22-12	Caliza "griotte"/Grioto Fm. and equivalents	limestone, red	43.443220	-4.864550	Carboniterous, Visean
ES-22-28	Caliza "griotte"/Grioto Fm. and equivalents	limestone, grey	43.209370	-5.091080	Carboniterous, Late Tournaisian to Visean
ES-22-27	Ermita Fm. and equivalents	limestone, grey, "Stinkkalk"	43.209840	-5.091160	Late Devonian
ES-22-34	Barrios Fm.	quartzite	43.426090	-5.075250	Early Ordovician, Early Tremadocian to Floian (Tramadoc-Arenig)
ES-22-15	Barrios Fm.	quartzite	43.442690	-4.867460	Early Ordovician, Early Tremadocian to Floian (Tramadoc-Arenig)
ES-22-18	Barrios Fm.	paraconglomerate	43.442770	-4.867470	Early Ordovician, Early Tremadocian to Floian (Tramadoc-Arenig)
ES-22-10	Barrios Fm.	quartzite	43.441390	-4.871020	Early Ordovician, Early Tremadocian to Floian (Tramadoc-Arenig)
ES-22-09	Barrios Fm.	quartzite	43.440910	-4.872510	Early Ordovician, Early Tremadocian to Floian (Tramadoc-Arenig)
ES-22-33	Oville Fm.	quartzite	43.424040	-5.080020	Middle to Late Cambrian (Drumian–Guzhangian)
ES-22-32	Lancara Fm.	dolostone	43.424210	-5.082350	Early to Middle Cambrian

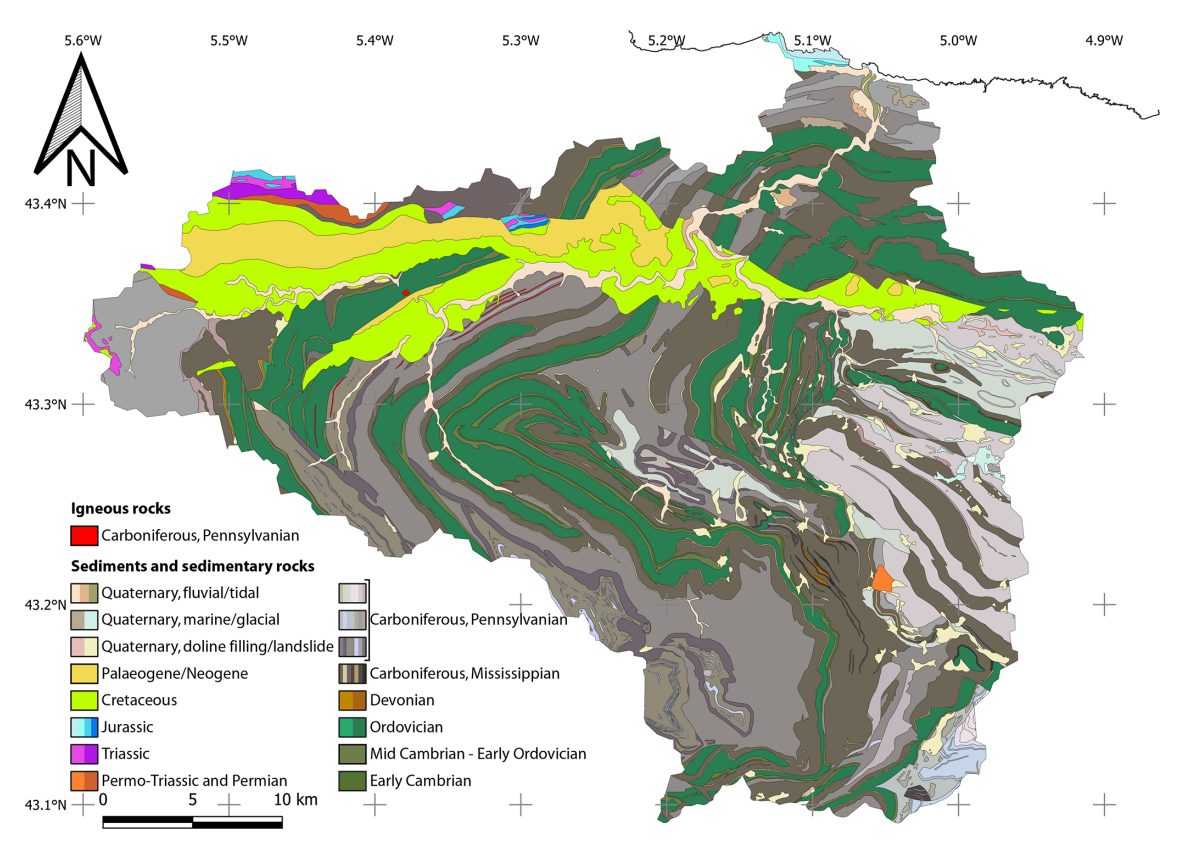
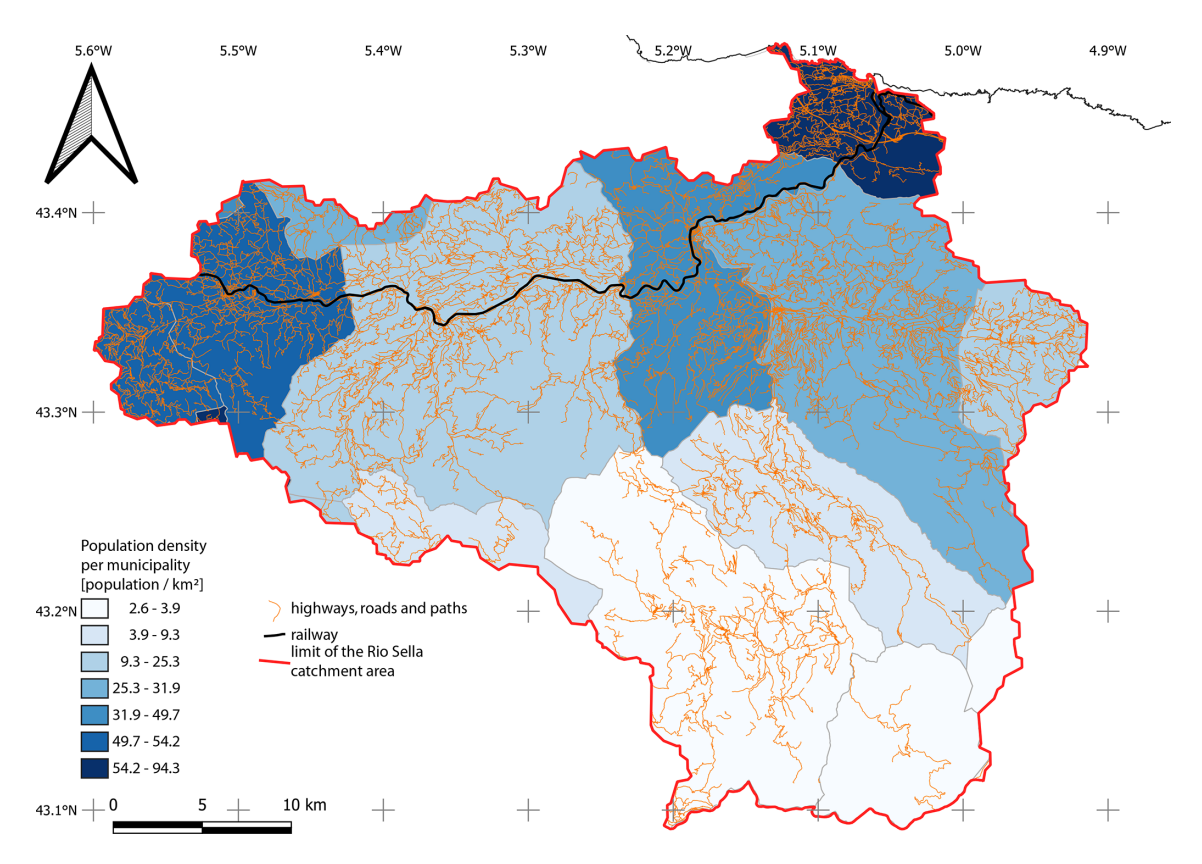


Figure 3. Geological overview of the Rio Sella catchment (derived from Alvarez-Marrón et al., 1990; Caride et al., 1975; Gervilla et al., 1973a, b; Hereida and Rodríguez Fernández, 1989; Hereida et al., 1990; Julivert and Navarro, 1984; Navarro and Leyva, 1986).

linearity = 0.2 mg). Subsequently, heavy mineral separation utilising LST (sodium heteropolytungstate) was employed at a density of 2.80–2.82 g cm<sup>-3</sup> to include all minerals of the tourmaline and amphibole groups with densities starting at around 2.82 g cm<sup>-3</sup>. Finally, the heavy mineral concentrates were re-weighed. Representative aliquots of all samples were mounted onto a stub object holder with adhered double-sided carbon tape (both from Plano). Special care was taken to avoid any mineral contacts. No further treatment was applied in order to retrieve the entire information on grain morphology. Prior to scanning electron microscope analyses, each sample was coated with a 5 nm thick carbon layer. Throughout the entirety of the preparation process, non-magnetic instruments were employed in order to preclude any potential bias in the magnetic heavy mineral fraction.

Images, morphology and elemental analyses were performed using an Apreo 2s (Thermo Fisher) scanning electron microscope (SEM) equipped with an ULTIM MAX 100 energy-dispersive X-ray spectrometer (EDS; Oxford Instruments). Data were acquired utilising the Oxford AZtec version 6.0 software, which enabled the quantification of grains, their elemental spectra and the measurement of morphometric characteristics, including length, width, shape and equivalent area circular diameter (ECD). The analysis was conducted at high vacuum (ca.  $1 \times 10^{-4} \, \mathrm{Pa}$ ), with an acceler-

ation voltage of 25 kV and a lower cut-off particle size of 5 µm. In order to ensure a minimum of at least 20 000 counts per analysis, the data acquisition time was set at 0.15 s per grain. Peak calibration was performed on elemental Ti and Mo. Stored element profiles for corresponding line series were employed for peak deconvolution. Each heavy mineral grain was individually identified and classified based on its elemental composition using an Excel-based in-house processing routine that was calibrated against 134 different reference materials of the most common minerals. The identified minerals were subsequently grouped as mica, garnet, amphibole, pyroxene, epidote, rutile, zircon, tourmaline and other transparent heavy minerals, in order to provide better comparability. The "other" group often makes up less than 10% of the total transparent heavy minerals by area (see below) but contains a large number of different minerals, the most abundant of which are indicated. As the detection limit of EDS analyses is approximately 0.1 to 0.5 mass per cent, very small elemental quantities in the grain size fractions are interpreted with caution. Tungsten and carbon were analysed and deconvoluted but were excluded from interpretation because they were used in the preparation processes (polytungstate and carbon tape). Dunkl et al. (2020) demonstrated that electron beam-based methods yield overall good identification results, especially if the heavy min-



**Figure 4.** Characteristics of anthropogenic activity in the Rio Sella catchment (data from Instituto Geográfico Nacional, 2024; Ministerio para la Transición Ecológica y el Reto Demográfico, 2023).

eral assemblage does not contain high proportions of polymorphs (which are not resolvable with electron beam methods, e.g. rutile/anatase/brookite, andalusite/kyanite/sillimanite) and chain silicates (which are difficult to discriminate with electron beam methods).

Heavy mineral grain mounts were additionally optically checked for polymorphs (TiO<sub>2</sub> and Al<sub>2</sub>SiO<sub>5</sub>).

Final results are presented as area per cent (area %) and grain counts (grain %) for equivalent circle diameter (ECD) of different size fractions (630–6.3, 630–200, 200–63, 63–20, 20–6.3 µm). The first mentioned method (area %) is deemed to be a more accurate representation of the actual heavy mineral proportions and is therefore recommended for future studies. It is calculated as a ratio of a specific mineral phase's area over the total area of all transparent heavy minerals. However, the latter method (grain %) was chosen in order to ensure comparability with previously published data. In general, those (sub)samples with less than 300 analysed grains (Table S1 in the Supplement) are interpreted with caution.

Although mica and dolomite are not a part of traditional heavy mineral studies, they are reported here because of their densities that match the criteria of heavy minerals (annite =  $3.33 \, \mathrm{g \, cm^{-3}}$ , "biotite" =  $2.81 \, \mathrm{to} \, 3.12 \, \mathrm{g \, cm^{-3}}$ , muscovite =  $2.76 \, \mathrm{to} \, 3.10 \, \mathrm{g \, cm^{-3}}$ , dolomite =  $2.85 \, \mathrm{g \, cm^{-3}}$  and

often higher; Gaines et al., 1997; Rösler, 1988). Plots of principal component analysis (PCA) and multidimensional scaling (MDS) were performed using the provenance package of Vermeesch et al. (2016) for R (version 4.2.2).

The identification of heavy anthropogenic particles (HAPs; here, all particles with a density of more than 2.80- $2.82 \,\mathrm{g \, cm^{-3}}$ , i.e. those anthropogenic particles in the heavy mineral fraction) focussed on those particles that show a distinctly different chemical composition from minerals, like typical metal alloys, e.g. bronze, brass, ferrocerium and different types of steel, as well as native metals like aluminium, lead, tin, zinc and copper. Particles with high amounts of rare earth elements (REEs) in non-natural concentrations and combinations are also regarded as being of anthropogenic origin. Furthermore, heavy glasses like bariumtitanate, whose natural equivalent is often close to the composition of the rare mineral benitoite, are among the identified HAPs. A further group of particles is characterised by very high quantities of iron (>> 75 %). That may correspond to different alloys of steel, which are characterised by very high amounts of Fe and additional metals but a very low abundance of O (Bradai et al., 2008; Nguyen et al., 2017; Ramachandra et al., 2005). Therefore, a separately listed class of particles with  $\gg 75\%$  Fe, here termed Fe++, could represent (partly oxidised) remnants of various steel alloys. As an analysis of oxygen from topographically different mineral particles can result in slightly shifted O values (e.g. edge effect on very small grains), particularly the smaller of the latter particles have to be interpreted with care. Following extensive analysis, it was determined that the presence of certain spherules indicated a likely anthropogenic origin. Due to their propensity for future automated identification, they have also been placed in a separate class.

Overall, the identification of HAPs in modern sediments (Fig. S1) is likely an estimate of minimum abundance, because maybe not all classes of HAPs are yet identified or known. First estimates of HAP concentrations in sediments are derived from the total number of HAPs in a weighed aliquot of the total heavy mineral fraction (whose amount of the total sediment was logged for each sample).

$$HAP \ per \ [g] \ sample = \frac{HAP}{HM_{aliquot} \ [g]} \cdot \frac{HM_{total} \ [g]}{sample_{total} \ [g]} \tag{1}$$

The calculation of relative uncertainties of the number of the total HAPs per gram sample is based on the reproducibility of the used balance at every weighing step and yields a mean of +13.2%/-18.8% and a median of +12.0%/-16.0%.

#### 4 Results

In this study, a total of 363 547 heavy mineral grains (opaques + transparent + dolomite) from 37 samples (15 modern sediments, 22 pre-Quaternary (meta)-sedimentites) were analysed, with special emphasis on the transparent heavy minerals. A general description of the samples is based on the entire grain size range with some remarks on significant grain-size-dependent changes in heavy mineral distribution in Sect. 4.1 and displayed in the respective figures. As the TiO<sub>2</sub> polymorphs rutile, anatase and brookite cannot be distinguished by EDS analysis, "traditional" microscopy revealed a very clear predominance of rutile. Therefore, the TiO<sub>2</sub> group minerals are termed "rutile" in the following text. Besides the transparent heavy mineral groups mica, garnet, amphibole, pyroxene, epidote, rutile, zircon and tourmaline, there are additional "other" heavy minerals. They mostly account for less than 10 area % of the transparent heavy minerals per sample and were mainly identified as and alusite/kyanite/sillimanite, apatite and staurolite, as well as occasionally topaz, monazite and titanite. At some localities, fluorite and barite occur abundantly but are not reported as single groups. Further details on the heavy mineral distribution of each sample are given in Table S1. HAPs are characterised further on.

#### 4.1 Heavy mineral characteristics of the samples

The total heavy mineral content differs significantly between the rock (0.45 wt. % with outlier sample ES-22-32, 0.26 wt. % without) and the modern sediment samples (1.38 wt. %). Looking at the opaque grains, the entire Cambrian and Ordovician samples are depleted in such miner-

als (2.85 area % of the entire heavy mineral fraction), while all other samples, except for Carboniferous limestone ES-22-26 and shale ES-22-19, show marked abundances, often reaching values around or even above 40 area % (average of all = 40.88 area %, Fig. S2). Dolomite, however, is abundant in just a few samples (ES-22-32, ES-22-26) and reaches significant values of about 15 area % or more of the entire heavy mineral concentrate in only five additional samples (ES-22-13, ES-22-30, ES-22-31, ES-22-35, Gijón bridge). In most of the analysed samples, the transparent heavy mineral fraction makes up the main heavy mineral group (Fig. S2).

# 4.1.1 Grain size distribution of selected heavy mineral groups

The grain-size-dependent distribution of certain transparent heavy minerals in sediments and sedimentary rocks is well known but not yet fully understood (Rittenhouse, 1943; Feil et al., 2024) and has also been documented in the Rio Sella catchment (Fig. 5). Although the length, width, area and ECD are logged for each single analysis and may be used in further studies, the grain size analyses presented here are focussed on mica, garnet, amphibole, pyroxene, epidote, rutile, zircon and tourmaline in the grain size fractions of 630–200, 200–63, 63–20 and 20–6.3 µm. Of these, results from the 630–200 µm fraction should be interpreted with caution due to low heavy mineral counts.

It becomes evident that mica grains show a clear trend in becoming more abundant in smaller grain size fractions. The same seems to be valid for garnet, except for some very large grains that are provided in modern sediments (Fig. 5). Similar patterns were found for amphibole and pyroxene, which are also abundant in the 630-200 µm fraction, decreasing in abundance in the 200-63 µm fraction and then increasing towards smaller grain sizes. At least in the studied samples, epidote seems to be absent in the 630-200 µm fraction and has a pronounced maximum of 63–20 µm. The grain size distribution of rutile is somehow different from all other mineral groups in this study. While the overall distribution seems to be nearly constant for 200-6.3 µm, the trends in modern sediments and the pre-Quaternary sedimentary rocks differ significantly. While rutile grains in modern sediments seem to decrease from 200-63 µm towards smaller grain sizes, the grain size distribution of rutile grains from pre-Quaternary sedimentary rocks resembles that of mica. Grain sizes of zircon are quite consistent throughout the sample set, showing an unequal distribution with a pronounced peak in the 200– 63 µm fraction. Finally, tourmaline shows a trend to mostly occur between 200 and 6.3 µm, with a less prominent peak at  $63-20 \, \mu m$ .

### 4.1.2 Distribution of transparent heavy minerals

Except for abundant dolomite, the oldest rock of this study, an Early to Middle Cambrian dolostone (ES-22-32), con-

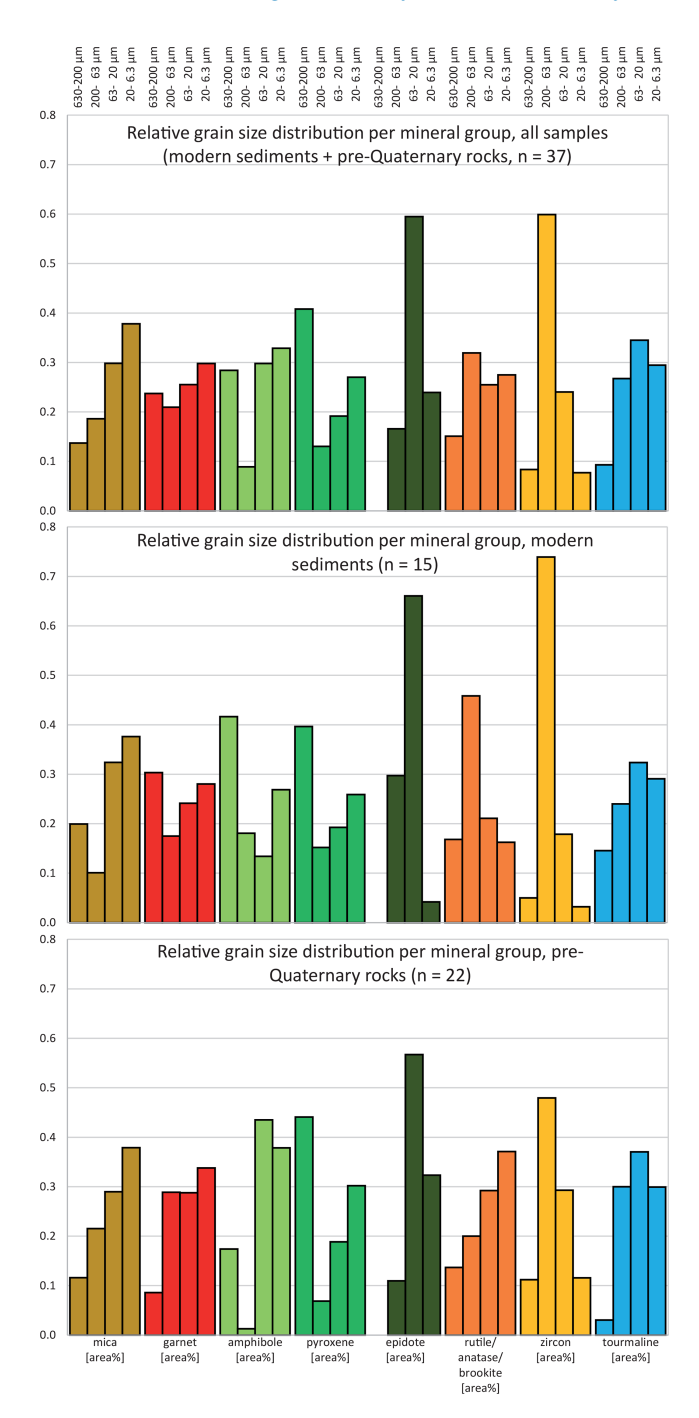


**Figure 5.** Relative grain size distribution (fractions 630–200, 200–63, 63–20 and 20– $6.3 \,\mu m$ ) of mica, garnet, amphibole, pyroxene, epidote, rutile, zircon and tourmaline for all samples (upper diagram), the modern sediments (middle diagram) and the pre-Quaternary samples (lower diagram).

tains only few heavy minerals, mainly concentrated in the  $< 200 \, \mu m$  fraction. These are mica, garnet, amphibole, rutile and, as a main constituent of the "other" group, apatite. All other heavy minerals occur only in small proportions. Stratigraphically overlying, the Middle to Late Cam-

brian siliciclastic sample ES-22-33 is characterised by abundant mica and apatite, as well as some amphibole, while the other transparent heavy minerals combine to less than 10 area % on average. The Ordovician samples ES-22-09, ES-22-10, ES-22-15, ES-22-18 and ES-22-34 are very similar to each other. Except for relatively high amounts of mica in ES-22-09 and ES-22-10, all these samples are composed mainly of rutile, zircon and tourmaline, making them a characteristic group in the studied catchment (Fig. 6). Late Devonian and Early Carboniferous (Visean) carbonate rocks (ES-22-11, ES-22-12, ES-22-14, ES-22-27, ES-22-28) also constitute a quite similar group of rocks concerning their heavy mineral composition. These strata contain high amounts of apatite and occasionally (ES-22-28) calciumsilicate that resemble the chemical composition of calicoolivine with only very little variance. Stratigraphically upsection (Navarro and Leyva, 1986), the amount of mica, garnet and rutile increases slightly. Additionally, sample ES-22-11 contains comparatively high amounts of pyroxene. ES-22-13 appears to be unique among the samples examined, containing mainly zircon and being the only "basement" sample with significant Al<sub>2</sub>SiO<sub>5</sub> minerals (and alusite, kyanite, sillimanite). Its smallest grain size fraction also contains garnet, amphibole, pyroxene and rutile but is devoid of zircon. Samples ES-22-25 and ES-22-26 contain too few heavy minerals for further interpretation other than that they do not provide such material to the modern drainage system. Late Carboniferous conglomerate and shale samples ES-22-19, ES-22-20, ES-22-21 and ES-22-22 are again quite similar concerning their heavy mineral spectra. These rocks contain abundant mica and garnet, while all other transparent heavy minerals barely add up to much more than 20 area % independent of their grain size fraction. The Late Carboniferous calcareous pelite ES-22-17 is a small isolated type of deposit outside the Rio Sella catchment but within the adjacent Rio de las Cabras o Bedón drainage area. Its heavy mineral content differs a lot from those of the aforementioned Late Carboniferous rocks as it includes plenty of apatite and baryte as main constituents, while the other transparent heavy mineral groups rarely account for more than 20 area % of each grain size fraction (Fig. 6). Jurassic rocks that are present in the lower reaches of Rio Sella are exemplarily studied by sample ES-22-35. Containing significant mica and garnet, this rock resembles the Late Carboniferous group, except for slightly higher amphibole and epidote. Finally, sample ES-22-37 is from a Cretaceous siliciclastic rock but sampled about 70 km east of Ribadesella. Therefore, it is likely not entirely representative for the Cretaceous of the Rio Sella catchment; however, given the homogeneity of Cretaceous transgressive sandstones in other parts of Europe (e.g. Gärtner et al., 2025), it may provide an idea about the potential heavy mineral signal. This sample contains abundant mica, rutile and tourmaline, whereas all other transparent heavy minerals add up to less than ca. 8 area %, independent of their grain size fraction.

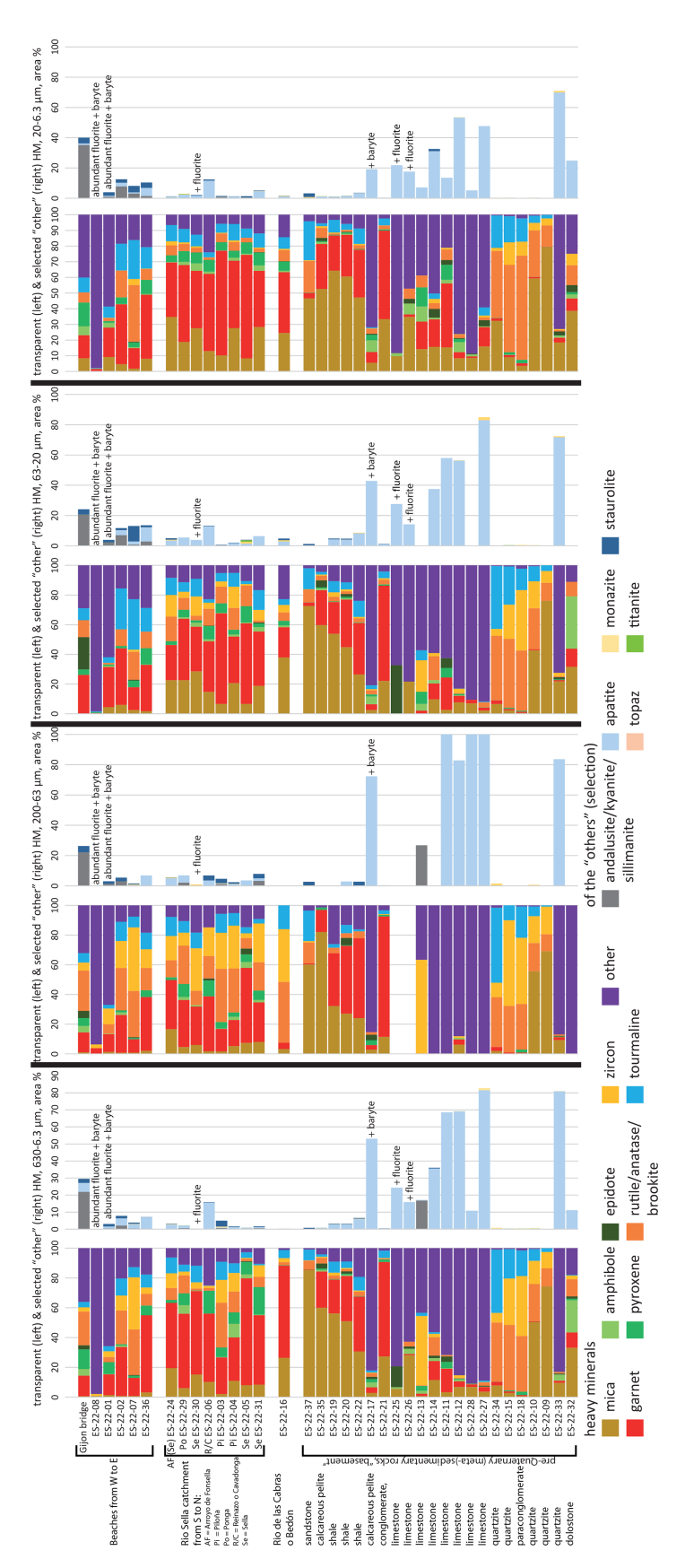


Figure 6. Summary of the heavy mineral spectra of each sample for the entire grain size spectrum (630–6.3  $\mu$ m) as well as for 200–63, 63–20 and 20–6.3  $\mu$ m.

The modern sediments of the Rio Sella catchment (ES-22-03, ES-22-04, ES-22-05, ES-22-06, ES-22-24, ES-22-29, ES-22-30, ES-22-31) are relatively similar in total heavy mineral content. They contain some mica, abundant garnet, sparse but consistent pyroxene and, except for samples ES-22-05, ES-22-06 and ES-22-30, significant zircon, tourmaline and rutile. All other heavy minerals are either occasional (amphibole, staurolite) or present at very low levels if not absent. The samples are also very similar in the 200–63, 63–20 and 20–6.3 µm fractions (Fig. 6). The one additional sample from the Rio Cabras o Bedón (ES-22-16) has a quite similar heavy mineral distribution to the other fluvial samples, which is likely because of similar lithology proportions.

Finally, the modern beach sediments (Gijón bridge, ES-22-01, ES-22-02, ES-22-07, ES-22-08 and ES-22-36) are all depleted in mica. ES-22-08 is different from all other beach samples, because its heavy minerals are mainly composed of fluorite and barite. Except for the Gijón bridge sample, which yields the highest amounts of andalusite, kyanite and sillimanite (as well as staurolite), amphibole, pyroxene and epidote are also scarce. In contrast, garnet is abundant, while rutile, zircon and tourmaline occur in variable values.

### 4.2 Heavy anthropogenic particles (HAPs)

Heavy anthropogenic particles are abundant in the fluvial sediments ranging between 58 and 4170 HAP  $\rm g^{-1}$  per sample including the Fe++ group that represents the most common particle group. The resulting average value is ca. 1220 HAP  $\rm g^{-1}$ . If ignoring the Fe++ group, the values range from 0 to 92 particles HAP  $\rm g^{-1}$  including 0 to 10 spherules per gram. In comparison, the beach samples contain far fewer HAPs in a range from 4 to 277 HAP  $\rm g^{-1}$  (average = ca. 63 HAP  $\rm g^{-1}$ ). Almost all potential HAPs of the beach samples belong to the Fe++ group, with very minor numbers of other HAPs in the Gijón bridge and ES-22-08 samples. Only the Gijón bridge sample contained a few glassy spherules accounting for about one spherule per gram of sediment.

#### 5 Discussion

Given the limited sample set examined, which may not be representative of the entire catchment, the following hypotheses are merely preliminary and require further data support to substantiate them. Despite the fact that samples ES-22-09 to ES-22-15 and ES-22-17, as well as ES-22-18, were obtained from the catchment of the adjacent Rio de las Cabras o Bedón, they are regarded as being also representative of the equivalent rocks within the Rio Sella catchment. However, the quantity of samples and heavy mineral grains analysed appears to be unparalleled in such small catchments and is therefore intended as a basis for future investigations.

Previous studies have shown that different rocks contain different groups and amounts of heavy minerals (Cascalho and Fradique, 2007; Garzanti and Andò, 2019; Morton and Hallsworth, 1994), although the often-cited statement that carbonate rocks do not supply heavy minerals is obviously not valid (e.g. Čeplak et al., 2023; Gärtner et al., 2017; this study). It is also well known that certain heavy minerals are less stable against chemical weathering (Garzanti et al., 2013; Pettijohn, 1941) and diagenetic dissolution (Garzanti et al., 2018; Morton and Hallsworth, 2007) than others. Garzanti and Andò (2007) consequentially state that heavy mineral signatures of detrital materials mirror at least the combined effects of the geology of the source region(s), sedimentary processes and digenesis. Furthermore, heavy minerals tend to occur in different grain size fractions (Frihy et al., 1995; Jin et al., 2021). However, this is not necessarily an effect of pure hydrodynamic sorting but could be a matter of specific parameters obviously controlling crystal (re-)growth parameters (e.g. Krippner et al., 2015; Poldervaart, 1956) in the source rocks and grain size inheritance (Feil et al., 2024), which is corroborated by the present study. Despite all variations and uncertainty for some processes, there is consensus that heavy minerals are a powerful tool for provenance studies and sediment routing (Garzanti and Andò, 2007; Morton, 1985).

# 5.1 Heavy mineral provenance of modern fluvial samples

Irrespective of their position in the catchment, the modern fluvial sediment samples have similar detrital heavy mineral signatures (Fig. 6). This is further supported by the PCA and MDS plots (Fig. 7) and suggests a proper mixing and sort of homogenisation of the studied detrital components. Compared to most of the siliciclastic rocks, the modern sediments show low amounts of mica. This characteristic is likely attributed to hydrodynamic fractionation (Komar et al., 1984; Sun et al., 2020) as mica of all grain sizes is present in several of the studied pre-Quaternary rocks and should thus not be overinterpreted in terms of potential host rocks within the catchment area. Furthermore, the fluvial samples contain distinct amounts of garnet, which is a principal constituent of the post-Middle Carboniferous rocks, i.e. sample ES-22-21 and younger. Concurrently, the ultra-stable heavy minerals zircon, tourmaline and rutile are present in abundance in the Ordovician siliciclastic rocks (Fig. 7). All fluvial samples show low, yet consistent, levels of pyroxene, a rare occurrence in all of the studied rocks within the Rio Sella catchment. At the current state of knowledge, the provenance of pyroxene continues to elude definitive identification, yet its ubiquity is a salient phenomenon. Finally, the modern fluvial samples are depleted in apatite, which is the prevailing accessory mineral in the majority of local carbonate rocks (Fig. 6). This observation merits a comprehensive discussion.

Notwithstanding the potential for bias in the apparent heavy mineral weights resulting from the local presence of dolomite (Fig. S2), aragonite (Alderton, 2021) and, on occasion, calcite, which has been observed to attain a maximum

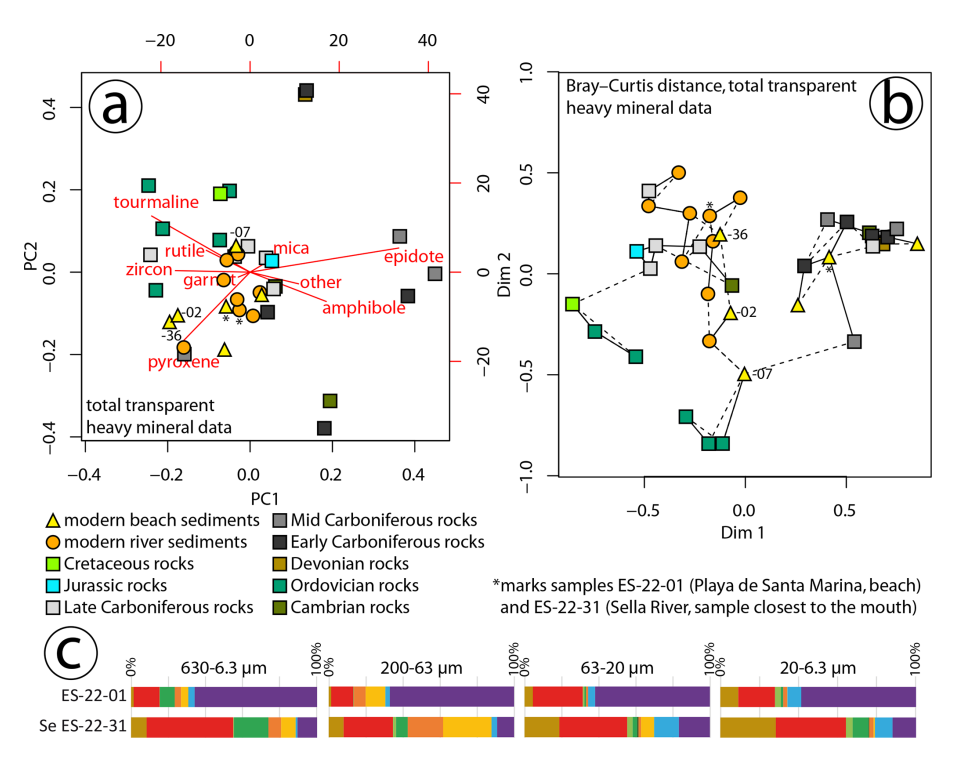


**Figure 7.** (a) Principal component analysis for all samples in this study (samples ES-22-02, ES-22-07 and ES-22-36 are identified by "-02", "-07" and "-36"). (b) Multidimensional scaling applying Bray–Curtis distance for all samples (samples ES-22-02, ES-22-07 and ES-22-36 are identified by "-02", "-07" and "-36"). (c) Comparison of sample ES-22-01 (beach, Ribadesella) with sample ES-22-31 (lower reaches of the Rio Sella). For the legend, see Fig. 6.

density of approximately 2.8 g cm<sup>-3</sup> (Rösler, 1988), the carbonate rocks exhibit a similar average percentage of heavy minerals by weight but lower mineral diversity compared to the studied siliciclastic rocks. The latter is in line with observations reported by Čeplak et al. (2023). Consequently, at least some of the carbonate rocks under consideration are theoretically capable of contributing significant quantities of heavy minerals to modern fluvial sediments. Others, like samples ES-22-25 and ES-22-26, as well as ES-22-11 and ES-22-28, yielded insufficient quantities of heavy minerals to be considered as detectable heavy mineral sources. Despite the spatial distribution of carbonate rocks, siliciclastic rocks and mixed lithologies approximating 2:1:1 (see above), a major signal of those carbonate rocks yielding sufficient numbers of heavy minerals is not reflected in the heavy mineral content of the modern fluvial sediments. This finding is deduced from the analysis of one of the most abundant heavy minerals in these carbonaceous lithologies, namely apatite, which is found in negligible quantities in fluvial sediments. An exception is sample ES-22-06, which was collected in a subcatchment dominated by calcareous rocks (Fig. 2). It is evident that, in this particular locale, the apatite is transferred to fluvial sediments. However, the question of its disappearance in the main stream(s) remains unresolved. Despite its relatively low resistance to chemical weathering, particularly in lower pH environments, the mineral exhibits notable sta-

bility during "physical" transport (Mange and Maurer, 1991) and can be transported over considerable distances in rivers (Zoleikhaei et al., 2016). It can be concluded that dissolution by low-pH stream water is also not a contributing factor, as the carbonate rocks have been shown to buffer the pH (Lin et al., 2023) at approximately 8. This is also valid in the lower reaches of the Rio Sella (Ovín Vega, 2014). Features visible in SEM images of single apatite grains resemble intense surficial pitting due to collisions (Fig. S3), which might result in the rapid fragmentation of larger grains and may explain the rapid decrease of this mineral group. The comparatively low specific density of apatite (ca. 3.1 to  $3.2 \,\mathrm{g \, cm^{-3}}$ ) may additionally result in hydrodynamic sorting, although this feature should then also be observable in mineral groups of similar density like tourmaline or many of the minerals in the amphibole group (Gaines et al., 1997; Rösler, 1988).

In conclusion, heavy minerals of the carbonate rocks may only be present in the adjacent fluvial sediments but are not transferred from tributaries to the river's main stream or mouth in a grain size between 630 and 6.3 µm. The vast majority of transparent heavy minerals apparently originates from Cambro–Ordovician (zircon, rutile, tourmaline, some mica) and post-Middle Carboniferous (garnet, mica) siliciclastic rocks. Pre-Quaternary siliciclastic rocks account for approximately one-quarter of the Rio Sella catchment, while siliciclastic parts in areas with mixed strata may account for

another ca. 12 %. Therefore, only a bit more than one-third of the outcropping rocks significantly contributes to the heavy mineral spectrum of the river.

### 5.2 Heavy mineral provenance of modern beach sediments

It seems to be consensus that the oceanic currents are the main factor of sediment transport along coastlines (Liu et al., 2008). However, even in small catchment areas it would be expected that the heavy mineral characteristics of beach sediments immediately at the river's mouth (ES-22-01) show some similarities with those of the lower course of the river itself (ES-22-31). Both of the samples show little similarity concerning their heavy mineral spectra throughout all grain size fractions (Fig. 7a, b, c). Thus, the amount of sediments transported by longshore currents directed to the east (Martínez et al., 2024) seems to overprint most of the river's input at this location.

Interestingly, the modern beach sediments along the northern coast of Spain show less similarity among each other than the modern fluvial sediments (Fig. 7a, b, c). This is in line with the previously published data of Flor (1978). Here, no large littoral cells, like those exemplary cells described by Garzanti et al. (2014), seem to exist, as the heavy mineral signal changes constantly with a large variance (Fig. 6; Flor, 1978). On the other hand, the heavy mineral signal does not seem to be immediately affected by the input of the rivers, as found for other systems (Gärtner et al., 2022).

In the case of the northern Spanish coast, the rocks that crop out at the shoreline seem to be the main entity for the heavy mineral signal of beach sediments. Despite individual characteristics, the three western samples - Gijón bridge, ES-22-08 and ES-22-01 - form one group in the MDS-plot (Fig. 7b), suggesting a comparably similar overall heavy mineral composition of the source rocks. The three eastern samples – ES-22-02, ES-22-07 and ES-22-36 – can also be loosely grouped. Looking at a geological overview map (Fig. 8), it becomes obvious that the general lithology changes immediately to the east of sampling locality ES-22-01. Accepting a very rapid effect of changing coastal lithologies would explain the observed phenomenon and would also explain the findings of Flor (1978). The immediacy of the input of local "marker minerals" is exemplarily illustrated by the high fluorite content of sample ES-22-08, sampled at the beach northeast of Bebes. Here, fluorite deposits are well known and were also mined to a certain extent, e.g. near the sampled beach (Pérez-Cejuela, 2009; Symons et al., 2017). Therefore, the comparatively high amount of detrital fluorite in beach sample ES-22-08, and maybe even in ES-22-01, can be explained by past mining activities and/or erosion in the close vicinity. Further examples are ES-22-02 and ES-22-07. Both of them are dominated by ultra-stable zircon, rutile and tourmaline, with little garnet and traces of apatite. In particular, the ultra-stable heavy minerals zircon, rutile and tourmaline characterise the Ordovician rocks (Fig. 6). The latter become abundant in the sampled area east of Ribadesella (ES-22-01). The sources of garnet may lie in the coastal hinterland and may represent the fluvial component. Nevertheless, this has to be proven by further sampling of strata cropping out along the coast. In any case, most of the Carboniferous rocks along this part of the coast are biogenic limestones (Martínez García, 1981), which are expected to be significantly depleted in non-calcitic/aragonitic minerals. This line of argument is challenged by the sample pair ES-22-37, a Cretaceous sandstone; and ES-22-36, which is the corresponding beach sand. They differ not only in their mica content, which is possibly depleted in the beach sand due to high affinity to hydrodynamic fractionation, but there are also further striking differences like very little zircon, amphibole and pyroxene in ES-22-37 compared to ES-22-36. At the current state, a mixing between sediments transported parallel to the coast and local material can be hypothesised for this particular locality.

# 5.3 Occurrence and transport of heavy anthropogenic particles (HAPs)

The investigation of anthropogenic particles and heavy metal concentrations in urban road dust or airborne material has been a subject of study for a considerable period (see Chrysakopoulou et al., 2023; Yang et al., 2010; Zhang et al., 2012). Furthermore, analogous particles have been identified in modern marine sediments (Hrong et al., 2009), thereby substantiating the hypothesis of their potential pervasive existence.

HAPs have been detected in all studied modern fluvial and beach samples (Table S1). Of the samples analysed, ES-22-03 and ES-22-24 exhibited the highest concentrations of total HAPs (if accepting Fe++ as anthropogenic in origin), with levels of 4170 and 3838 HAP  $g^{-1}$  of the untreated sample, as illustrated in Fig. 9. It is noteworthy that both samples were collected in close proximity to main roads; however, this is a common occurrence for most samples obtained from the Rio Sella catchment and thus does not provide a definitive explanation for the elevated figures observed. For sample ES-22-03, no plausible explanation can be proffered for such elevated HAP numbers at this time, on account of the absence of either particle-emitting hotspots, such as junctions (Li et al., 2004), curves, industrial complexes or larger settlements. In close proximity to the sampling site is a farmstead and a railway crossing situated beneath the road. The railway runs parallel to the road until Ribadesella, along which samples ES-22-04, ES-22-05 and ES-22-31 were taken at comparable sites but yield significantly fewer HAPs. Consequently, the railway cannot be identified as the primary source for the local increase in HAP concentration.

In contrast, ES-22-24 is located at the headwaters of the Rio Sella but contains abundant HAPs even apart from Fe++. As the particles were collected upstream of a small bridge on

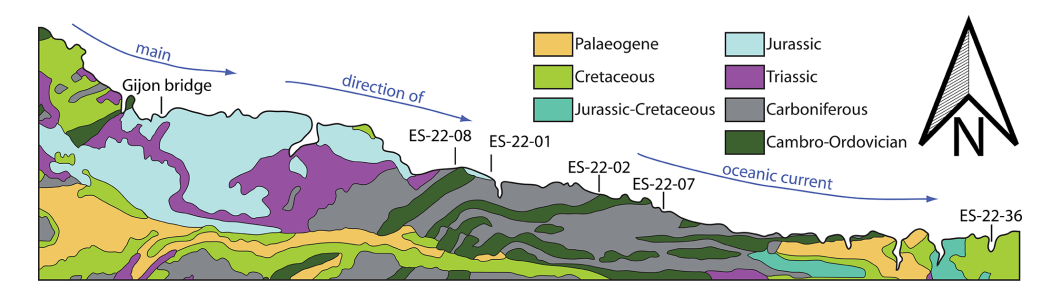


Figure 8. Sketch map of the main geological features along the northern Spanish coast between Gijón and Torrelavega (based on Rodríguez Fernández et al., 2015).

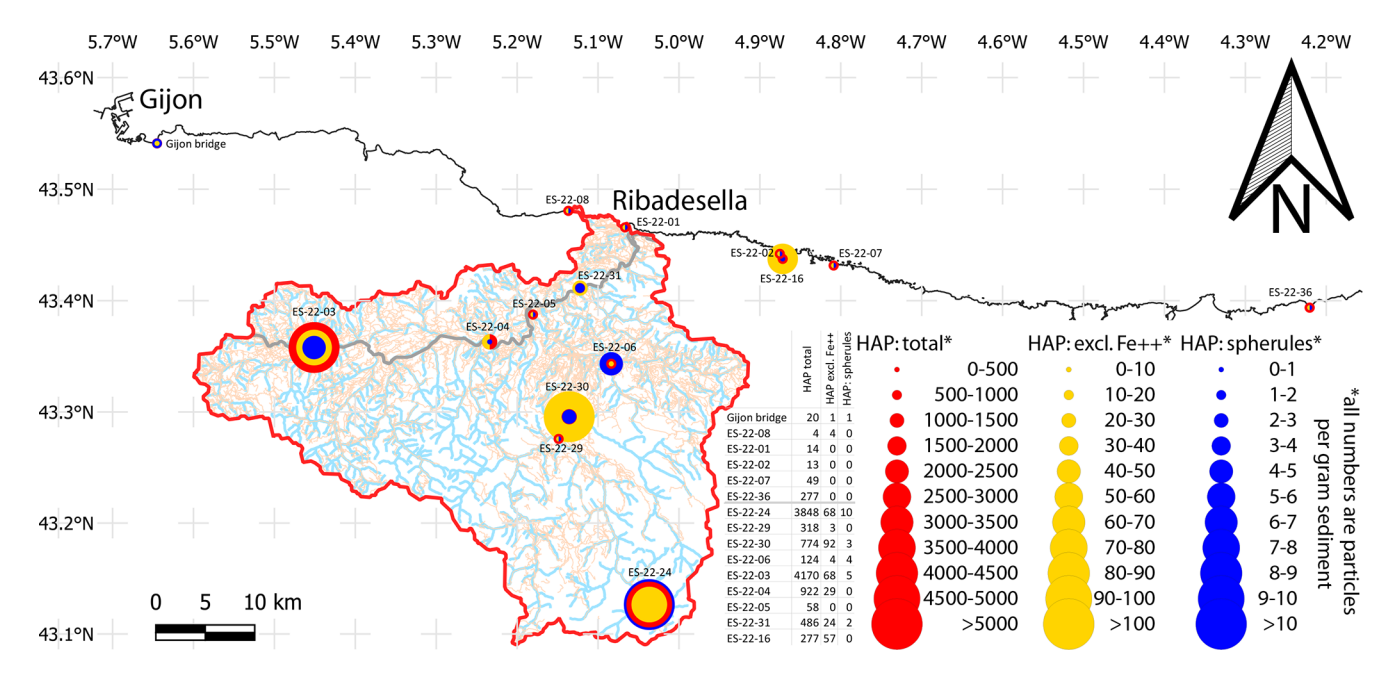


Figure 9. Distribution of HAPs in the studied modern sediment samples.

a little-used single-lane road, it is interpreted that they were added to the sediments elsewhere. However, a mere few hundred metres above this point, the busy main road that also traverses the creek leads over the pass to the south. The presence of numerous hairpin bends (Fig. 4) in the area may necessitate increased braking by vehicles, thereby potentially leading to elevated levels of HAP emissions (Adamiec et al., 2016). This phenomenon, occurring in a relatively unpopulated region, warrants further investigation to understand its impact on the environment. This observation is further corroborated by the findings of sample ES-22-30, which was collected from Rio Sella in a less-populated area. With the exception of its proximity to the primary thoroughfare, there are few discernible discrepancies compared to the closely taken sample ES-22-29, which exhibited significantly diminished HAPs. It has to be noted that the number of HAPs decreases downstream and does not even get higher in urban areas like Ribadesella. An exception is sample ES-22-16, taken in the lower reaches of the Rio de las Cabras o Bedón in proximity of a large highway bridge, which might explain the significantly elevated values of Fe++. Generally, there is no downstream trend of changing HAP group ratios at all. In contrast, the modern beach sediments seem to be depleted in HAPs. At the current state of knowledge, the reason for this phenomenon remains unclear. However, it is plausible that destruction due to physical weathering during transport or chemical reactions may be plausible scenarios leading to the HAP decrease in modern beach sediments. The hypothesis of a grain size or sorting effect cannot be discounted but seems improbable given that the finer grain size fractions of modern beach sediments were also examined at comparable grain numbers. By contrast, the different heavy mineral composition of beach sediments compared with those of the Rio Sella should not affect HAP abundance, since the distribution of all anthropogenic materials should be independent of sediment mineral composition.

### 6 Conclusion

This study, albeit preliminary, demonstrates the significant impact of siliciclastic rocks on the heavy mineral spectrum in small mountainous catchment areas. Despite the fact that only approximately one-third of the total Rio Sella catchment area is composed of siliciclastic rocks, these rocks are responsible for the majority of heavy mineral deposits present at the river's mouth. Meanwhile, the presence of heavy mineral signals of carbonate rocks appears to be confined to subcatchments, where they prevail as the predominant lithological feature.

Upon reaching the sea, the mineral signals indicative of small mountainous rivers in northern Spain become obscured by sediments that are transported by longshore currents. The mineralogical data obtained from the study indicate that the mineralogical composition of beach sands is predominantly influenced by the locally outcropping rock formations along the coast, rather than by the mineralogical composition of the material provided by the small mountainous rivers in the region. This has consequences for all studies attempting to obtain information on catchments and hinterlands by sampling only small- to medium-sized river mouths. It is also possible that the consequences may extend to similar studies in large river systems.

Finally, every modern sediment sample exhibited occurrences of heavy anthropogenic particulate matter, referred to as the HAPs. Given the very limited knowledge of HAPs, the characterisation of this group of anthropogenic particles has not yet reached the level of microplastics, and therefore further investigation is required to achieve proper classification in future studies. The majority of these particles, which can amount to several thousand per gram of sediment, are characterised by their notably elevated iron content. This renders them possible remnants of steel that are at various stages of disintegration. Notwithstanding the aforementioned group, the total HAP count in sediments can exceed 90 particles per gram. Consequently, it appears prudent to augment existing research endeavours with the objective of obtaining more precise estimates of the quantities, velocities and origins of such particles and to elucidate their potential environmental ramifications.

**Data availability.** All data can be found in the Supplement accompanying this publication.

**Supplement.** The supplement related to this article is available online at https://doi.org/10.5194/egqsj-74-281-2025-supplement.

**Author contributions.** AG: conceptualisation (lead), data curation, formal analysis, investigation, methodology, resources, supervision, validation, visualisation and writing (original draft preparation).

ration). AS: conceptualisation (supporting), validation and writing (original draft preparation).

**Competing interests.** The contact author has declared that none of the authors has any competing interests.

**Disclaimer.** Publisher's note: Copernicus Publications remains neutral with regard to jurisdictional claims made in the text, published maps, institutional affiliations, or any other geographical representation in this paper. While Copernicus Publications makes every effort to include appropriate place names, the final responsibility lies with the authors. Views expressed in the text are those of the authors and do not necessarily reflect the views of the publisher.

**Special issue statement.** This article is part of the special issue "Archives of Quaternary river basin erosion". It is a result of the International Symposium on Archives of Quaternary River Basin Erosion, Galera, Andalusia, Spain, 6–10 April 2024.

**Acknowledgements.** We thank Gabriel Gutiérrez-Alonso and an anonymous reviewer for their thoughtful suggestions, which helped to improve the paper. Furthermore, we would like to thank Mara and Albin for their patience, support and interest during the sampling process.

Review statement. This paper was edited by Thomas Kolb and reviewed by Gabriel Gutiérrez-Alonso and one anonymous referee.

### References

Adamiec, E., Jarosz-Krzemińska, E., and Wieszała, R.: Heavy metals from non-exhaust vehicle emissions in urban and motorway road dusts, Environ. Monit. Assess., 188, 369, https://doi.org/10.1007/s10661-016-5377-1, 2016.

Alderton, D.: Carbonates (Ca, Mg, Fe, Mn), in: Encyclopedia of Geology, edited by: Elias, S. A., 382–394, https://doi.org/10.1016/b978-0-08-102908-4.00088-6, 2021.

Alvarez-Marrón, J., Pérez-Estaún, A., Aller Manrique, J., Hereida, N.: Geological map of Sheet no. 79 14-6 (Puebla de Lillo), Geological Map of Spain scale 1:50000, Second Series (MAGNA), Instituto Geológico y Minero de España (IGME) for consultation (data), https://info.igme.es/cartografiadigital/geologica/Magna50Hoja.aspx?language=es&id=79 (last access: 11 November 2025), 1990.

Aramburu, C. I. and García-Ramos, J. C.: La sedimentación cambro-ordovícica en la Zona Cantábrica (NO de España), Trab. Geol., 19, 45–73, https://reunido.uniovi.es/index.php/ TDG/article/view/2869 (last access: 11 November 2025), 1993.

Avanzini, M., García-Ramos, J. C., Lires, J., Piñuela, L., and Lockley, M. G.: Crocodylomorph Tracks from the Late Jurassic of Asturias (Spain), Ichnos, 14, 143–153, https://doi.org/10.1080/10420940601010943, 2007.

- Bahamonde, J. R., Colmenero, J. R., and Vera, C.: Growth and demise of Late Carboniferous carbonate platforms in the eastern Cantabrian Zone, Asturias, northwestern Spain, Sed. Geol., 110, 99–122, https://doi.org/10.1016/S0037-0738(96)00076-0, 1997.
- Blanco-Ferrera, S., Cózar, P., and Sanz-López, J.: Development of a Mississippian–Lower Pennsylvanian isolated carbonate platform within the basinal griotte facies of the Cantabrian Mountains, NW Spain, Facies, 67, 21, https://doi.org/10.1007/s10347-021-00629-w, 2021.
- Borrego, A. G., López García, A., and Merino-Tomé, O.: Petrographic and geochemical characterization of organic-rich Mississippian black shales in the north of Spain: Vegamián Formation, Cantabrian Zone, Int. J. Coal Geol., 190, 126–145, https://doi.org/10.1016/j.coal.2017.08.012, 2018.
- Bradai, M. A., Braccini, M., Ati, A., Bounar, N., and Benabbas, A.: Microstructure and adhesion of 100Cr6 steel coatings thermally sprayed on a 35CrMo4 steel substrate, Surf. Coat. Techn., 202, 4538–4543, https://doi.org/10.1016/j.surfcoat.2008.04.039, 2008
- Caride, C., Marcos, A., Gervilla, M., Ortuño, G., and Velando, F.: Geological map of Sheet no. 53 13-5 (Mieres), Geological Map of Spain scale 1:50000, Second Series (MAGNA), Instituto Geológico y Minero de España (IGME) for consultation (data), https://info.igme.es/cartografiadigital/geologica/Magna50Hoja.aspx?language=es&id=53 (last access: 11 November 2025), 1975.
- Cascalho, J. and Fradique, C.: The sources and hydraulic sorting of heavy minerals in the northern Portuguese continental margin, Dev. Sed., 58, 75–110, https://doi.org/10.1016/S0070-4571(07)58003-9, 2007.
- Čeplak, B., Miler, M., Zupančič, N., and Jarc, S.: Heavy minerals as indicators of source material in soils on carbonates, Geoderma Regional, 35, e00735, https://doi.org/10.1016/j.geodrs.2023.e00735, 2023.
- Chrysakopoulou, C., Vogiatzis, D., Drakoulis, A., Papadopoulou, L., and Kantiranis, N.: Heavy Metal Load in Airborne Magnetic Particles from Anthropogenic Activities in a Contaminated Area in Northern Greece and Their Environmental Impact, Envir. Sci. Proc., 26, 212, https://doi.org/10.3390/environsciproc2023026212, 2023.
- Colmenero, J. R.: Estratigrafía y Sedimentología de las Areniscas del Devónico Superior de la Zona Cantábrica (Asturias, León), Doctoral dissertation, PhD Thesis, Universidad de Oviedo, 280 pp., 1976.
- Dunkl, I., von Eynatten, H., Andò, S., Lünsdorf, K., Morton, A., Alexander, B., Aradi, L., Augustsson, C., Bahlburg, H., Barbarano, M., Benedictus, A., Berndt, J., Bitz, I., Boekhout, F., Breitfeld, T., Cascalho, J., Costa, P. J. M., Ekwenye, O., Fehér, K., Flores-Aqueveque, V., Führing, P., Giannini, P., Goetz, W., Guedes, C., Gyurica, G., Hennig-Breitfeld, J., Hülscher, J., Jafarzadeh, M., Jagodziński, R., Józsa, S., Kelemen, P., Keulen, N., Kovacic, M., Liebermann, C., Limonta, M., Lužar-Oberiter, B., Markovic, F., Melcher, F., Georgina Miklós, D., Moghalu, O., Mounteney, I., Nascimento, D., Novaković, T., Obbágy, G., Oehlke, M., Omma, J., Onuk, P., Passchier, S., Pfaff, K., Pinto Lincoñir, L., Power, M., Razum, I., Resentini, A., Sági, T., Salata, D., Salgueiro, R., Schönig, J., Sitnikova, M., Sternal, B., Szakmány, G., Szokaluk, M., Thamó-Bozsó, E., Tóth, Á., Tremblay, J., Verhaegen, J., Villaseñor, T., Wagreich, M.,Wolf, A.,

- and Yoshida, K: Comparability of heavy mineral data The first interlaboratory round robin test, Earth Sci. Rev., 103210, https://doi.org/10.1016/j.earscirev.2020.103210, 2020.
- Feil, S., von Eynatten, H., Dunkl, I., Schönig, J., and Lünsdorf, N. K.: Inherited Grain-Size Distributions: Effect on Heavy-Mineral Assemblages in Modern and Ancient Sediments, J. Geophys. Res. Earth Surf., 129, e2023JF007356, https://doi.org/10.1029/2023JF007356, 2024.
- Fernández Irigoyen, J. and Ruiz Fernández J.: Prospección geoarqueológica de las terrazas fluviales del río Sella (Oriente de Asturias): el yacimiento de El Caxili, Rev. C. & G., 22, 173–187, http://hdl.handle.net/10651/22881 (last access: 11 November 2025), 2008.
- Fernández Irigoyen, J., Ruiz Fernández, J., and Fernández Fernández, J.: Estudio geoarqueológico de terrazas fluviales en el Oriente de Asturias: el Paleolítico inferior y medio del Valle del Sella, I Congreso de Estudios Asturianos, 2, 33–53, ISBN: 978-84-87212-46-8, 978-84-87212-48-2, 2006.
- Flor, G.: Relación entre la distribución de sedimentos y la circulación costera en la región del Cabo Peñas, Trab. Geol. 10, 183–195, https://reunido.uniovi.es/index.php/TDG/article/view/2715 (last access: 11 November 2025), 1978.
- Frihy, O. E., Lotfy, M. F., and Komar, P.: Spatial variations in heavy minerals and patterns of sediment sorting along the Nile delta, Egypt. Sed. Geol., 97, 33–41, https://doi.org/10.1016/0037-0738(94)00135-H, 1995.
- Gaines, R. V., Skinner, H. C. W., Foord, E. E., Mason, B., and Rosenzweig, A.: Dana's New Mineralogy, John Wiley & Sons, 8th edn., 1819 pp., ISBN 9780471193104, 1997.
- Gärtner, A., Linnemann, U., and Hofmann, M.: The provenance of northern Kalahari Basin sediments and growth history of the southern Congo Craton reconstructed by U–Pb ages of zircons from recent river sands, Int. J. Earth Sci., 103, 579–595, https://doi.org/10.1007/s00531-013-0974-5, 2014.
- Gärtner, A., Youbi, N., Villeneuve, M., Sagawe, A., Hofmann, M., Mahmoudi, A., Boumehdi, M. A., and Linnemann, U.: The zircon evidence of temporally changing sediment transport the NW Gondwana margin during Cambrian to Devonian time (Aoucert and Smara areas, Moroccan Sahara), Int. J. Earth Sci., 106, 2747–2769, https://doi.org/10.1007/s00531-017-1457-x, 2017.
- Gärtner, A., Hofmann, M., Zieger, J., Sagawe, A., Krause, R., Stutzriemer, M., Gesang, S., Gerdes, A., Marko, L., Lana, C., and Linnemann, U.: Implications for sedimentary transport processes in southwestern Africa: a combined zircon morphology and age study including extensive geochronology databases, Int. J. Earth Sci., 111, 767–788, https://doi.org/10.1007/s00531-021-02146-1, 2022.
- Gärtner, A., Niebuhr, B., Breitfeld, H. T., Rösel, D., Schulze, M. C., and Wilmsen, M.: Multi-proxy provenance study of sandstones from the northern Bohemian Cretaceous Basin (Germany, Czechia) focused on tourmaline, rutile and garnet, Cret. Res., 177, 106203, https://doi.org/10.1016/j.cretres.2025.106203, 2025.
- Garzanti, E. and Andò, S.: Heavy mineral concentration in modern sands: implications for provenance interpretation, Dev. Sed., 58, 517–545, https://doi.org/10.1016/S0070-4571(07)58020-9, 2007.

- Garzanti, E. and Andò, S.: Heavy Minerals for Junior Woodchucks, Minerals, 9, 148, https://doi.org/10.3390/min9030148, 2019.
- Garzanti, E., Padoan, M., Andò, S., Resentini, A., Vezzoli, G., and Lustrino, M.: Weathering and relative durability of detrital minerals in equatorial climate: Sand petrology and geochemistry in the East African Rift, J. Geol., 121, 547–580, https://doi.org/10.1086/673259, 2013.
- Garzanti, E., Vermeesch, P., Andò, S., Lustrino, M., Padoan, M., and Vezzoli, G.: Ultra-long distance littoral transport of Orange sand and provenance of the Skeleton Coast Erg (Namibia), Marine Geol., 357, 25–36, https://doi.org/10.1016/j.margeo.2014.07.005, 2014.
- Garzanti, E., Andò, S., Limonta, M., Fielding, L., and Najman, Y.: Diagenetic control on mineralogical suites in sand, silt, and mud (Cenozoic Nile Delta): Implications for provenance reconstructions, Earth-Sci. Rev., 185, 122–139, https://doi.org/10.1016/j.earscirev.2018.05.010, 2018.
- Gervilla, M., Pignateli, R., Baron, A., Coma, J. E., Felgueroso, C., Ramírez del Pozo, J., and Giannini, G.: Geological map of Sheet no. 29 13-4 (Oviedo), Geological Map of Spain scale 1:50 000, Second Series (MAGNA), Instituto Geológico y Minero de España (IGME) for consultation (data), https://info.igme.es/cartografiadigital/geologica/Magna50Hoja.aspx?language=es&id=29 (last access: 11 November 2025), 1973a.
- Gervilla, M., Beroiz, C., Pignateli, R., Baron, A., Coma, J. E., Felguroso, C., Ramírez del Pozo, J., and Giannini, G.: Geological map of Sheet no. 30 14-4 (Villaviciosa), Geological Map of Spain scale 1:50000, Second Series (MAGNA), Instituto Geológico y Minero de España (IGME) for consultation (data), https://info.igme.es/cartografiadigital/geologica/Magna50Hoja.aspx?language=es&id=30 (last access: 11 November 2025), 1973b.
- Gervilla, M., Beroiz, C., Pignateli, R., Baron, A., Coma, J. E., Felguroso, C., Ramírez del Pozo, J., and Giannini, G.: Mapa Geológico de España, E, 1:50 000, notices to sheet 30, Villaviciosa, 1–54, https://info.igme.es/cartografiadigital/datos/magna50/memorias/MMagna0030.pdf (last access: 11 November 2025), 1973c.
- González-Fernández, B., Menéndez-Casares, E., Vicedo, V., Aramburu, C., and Caus, E.: New insights about the Upper Jurassic Lower Cretaceous sedimentary successions from Asturias (NW Iberian Peninsula), J. Iber. Geol., 40, 409–430, https://doi.org/10.5209/rev\_JIGE.2014.v40.n3.43078, 2014.
- Gutiérrez-Alonso, G., Fernández-Suárez, J., Gutiérrez-Marco, J. C., Corfu, F., Murphy, J. B., and Suárez, M.: U-Pb depositional age for the upper Barrios Formation (Armorican Quartzite facies) in the Cantabrian zone of Iberia: Implications for stratigraphic correlation and paleogeography, Geol. Soc. Am. SP., 423, 287–296, https://doi.org/10.1130/2007.2423(13), 2007.
- Hereida, N. and Rodríguez Fernández, L. R.: Geological map of Sheet no. 54 14-5 (Rioseco), Geological Map of Spain scale 1:50 000, Second Series (MAGNA), Instituto Geológico y Minero de España (IGME) for consultation (data), https://info.igme.es/cartografiadigital/geologica/Magna50Hoja.aspx?language=es&id=54 (last access: 11 November 2025), 1989.
- Hereida, N., Rodríguez Fernández, L. R., Suárez, A., Alvarez Marrón, J.: Geological map of Sheet no. 80 15-6 (Burón),

- Geological Map of Spain scale 1:50000, Second Series (MAGNA), Instituto Geológico y Minero de España (IGME) for consultation (data), https://info.igme.es/cartografiadigital/geologica/Magna50Hoja.aspx?language=es&id=80 (last access: 11 November 2025), 1990.
- Hrong, C.-S., Huh, C.-A., Chen, K.-H., Hang, P.-R., Hssiung, K.-H., and Lin, H.-L.: Air pollution history elucidated from anthropogenic spherules and their magnetic signatures in marine sediments offshore of Southwestern Taiwan, J. Marine Sys., 76, 468–478, https://doi.org/10.1016/j.jmarsys.2007.09.014, 2009.
- Instituto Geográfico Nacional: Transport 2024, http://www.ign.es/ web/ign/portal/cbg-redes-transporte (last access: 11 November 2025), 2024.
- Jin, B., Wang, M., and Yue, W.: Comparative analysis of heavy mineral characteristics of sediments from the Huanghe River and the Changjiang River based on the multiplewindow grain size strategy, Cont. Shelf Res., 216, 104326, https://doi.org/10.1016/j.csr.2020.104326, 2021.
- Jing, Y., Zhao, Q., Lu, M., Wang, A., Yu, J., Liu, Y., and Ding, S.: Effects of road and river networks on sediment connectivity in mountainous watersheds, Sci. Total Envir., 826, 154189, https://doi.org/10.1016/j.scitotenv.2022.154189, 2022.
- Julivert, M. and Navarro, D.: Geological map of Sheet no. 55 15-5 (Beleño), Geological Map of Spain scale 1:50 000, Second Series (MAGNA), Instituto Geológico y Minero de España (IGME) for consultation (data), https://info.igme.es/cartografiadigital/geologica/Magna50Hoja.aspx?language=es&id=32 (last access: 11 November 2025), 1984.
- Key, A. J. M., Jarić, I., and Roberts, D. L.: Modelling the end of the Acheulean at global and continental levels suggests widespread persistence into the Middle Palaeolithic, Hum. Soc. Sci Comm., 8, https://doi.org/10.1057/s41599-021-00735-8, 2021.
- Komar, P. D., Baba, J., and Cui, B.: Grain-Size Analyses of Mica within Sediments and the Hydraulic Equivalence of Mica and Quartz, J. Sed. Petrol., 59, 1379–1391, https://doi.org/10.1306/212F85E4-2B24-11D7-8648000102C1865D, 1984.
- Korup, O.: Earth's portfolio of extreme sediment transport events, Earth Sci. Rev., 112, 115–125, https://doi.org/10.1016/j.earscirev.2012.02.006, 2012.
- Krippner, A., Meinhold, G., Morton, A., Russell, E., and von Eynatten, H.: Grain-size dependence of garnet composition revealed by provenance signatures of modern stream sediments from the western Hohe Tauern (Austria), Sed. Geol. 321, 25–38, https://doi.org/10.1016/j.sedgeo.2015.03.002, 2015.
- Larsen, I. J., Montgomery, D. R., and Greenberg, H. M.: The contribution of mountains to global denudation, Geology, 42, 527–530, https://doi.org/10.1130/G35136.1, 2014.
- Li, X., Lee, S., Wong, S., Shi, W., and Thornton, I.: The study of metal contamination in urban soils of Hong Kong using a GIS-based approach, Envir. Poll., 129, 113–124, https://doi.org/10.1016/j.envpol.2003.09.030, 2004.
- Lin, K., Yu, T., Ji, W., Li, B., Wu, Z., Liu, X., and Li, C.: Carbonate rocks as natural buffers: Exploring their environmental impact on heavy metals in sulfide deposits, Eviron. Poll., 336, 122506, https://doi.org/10.1016/j.envpol.2023.122506, 2023.
- Liu, J. P., Liu, C. S., Xu, K. H., Milliman, J. D., Chiu, J. K., and Lin, S. W.: Flux and fate of small mountainous rivers de-

- rived sediments into the Taiwan Strait, Marine Geol., 256, 65–76, https://doi.org/10.1016/j.margeo.2008.09.007, 2008.
- López, I. and Pardo, M.: Tourism versus nature conservation: reconciliation of common interests and objectives an analysis through Picos de Europa National Park, J. Mt. Sci., 15, 2505–2516, https://doi.org/10.1007/s11629-018-4943-0, 2018.
- López-Gómez, J., Alonso-Azcárate, J., Arche, A., Arribas, J., Fernández Barrenechea, J., Borruel-Abadía, V., Bourquin, S., Cadenas, P., Cuevas, J., de la Horra, R., Bienvenido Díez, J., Escudero-Mozo, M. J., Fernández-Viejo, G., Galán-Abellán, B., Galé, C., Gaspar-Escribano, J., Aguilar, J. G., Gómez-Gras, D., Goy, A., Gretter, N., Heredia Carballo, N., Lago, M., Llorte, J., Luque, J., Márquez, L., Márquez-Aliaga, A., Martín-Algarra, A., Martín-Chivelet, J., Martín-González, F., Marzo, M., Mercedes-Martín, R., Ortí, F., Pérez-López, A., Pérez-Valera, F., Pérez-Valera, J. A., Plasenica, P., Ramos, E., Rodríguez-Méndez, L., Ronchi, A., Salas, R., Sánchez-Fernández, D., Sánchez-Moya, Y., Sopeña, A., Suárez-Rodríguez, Á., Tubia, J. M., Ubide, T., Valero Garcés, B., Vargas, H., and Viseras, C.: Permian-Triassic Rifting Stage, in: The Geology of Iberia: A Geodynamic Approach, edited by: Quesada, C. and Oliveira, J. T. Regional Geology Reviews, 29-112, https://doi.org/10.1007/978-3-030-11295-0\_3, 2019.
- Mange, M. A. and Maurer, H. F. W.: Schwerminerale in Farbe, Enke, Stuttgart, 148 pp., ISBN: 3-432-98781-1, 978-3-432-98781-1, 1991.
- Martínez, J., García-Ladona, E., Ballabera-Poy, J., Isern-Fontanet, J., González-Motos, S., Allegue, J. M., and Gonzalez-Haro, C.: Atlas of surface currents in the Mediterranean and Canary-Iberian-Biscay waters, J. Oper. Oceanogr., 17, 40–62, https://doi.org/10.1080/1755876X.2022.2102357, 2024.
- Martínez García, E.: Geological map of Sheet no. 32 16-4 (Llanes), Geological Map of Spain scale 1:50 000, Second Series (MAGNA), Instituto Geológico y Minero de España (IGME) for consultation (data), https://info.igme.es/cartografiadigital/geologica/Magna50Hoja.aspx?language=es&id=32 (last access: 11 November 2025), 1981.
- Milliman, J. D. and Syvitski, J. P. M.: Geomorphic/Tectonic Control of Sediment Discharge to the Ocean: The importance of Small Mountainous Rivers, J. Geol., 100, 525–544, https://doi.org/10.1086/629606, 1992.
- Ministerio para la Transición Ecológica y el Reto Demográfico: Population density, https://www.mapama.gob.es/app/descargas/descargafichero.aspx?f=Densidad\_Poblacion\_2023.zip (last access: 11 November 2025), 2023.
- Misset, C., Recking, A., Legout, C., Valsangkar, N., Bodereau, N., Zanke, S., Poirel, A., and Borginet, L.: The Dynamics of Suspended Sediment in a Typical Alpine Alluvial River Reach: Insight From a Seasonal Survey, Water Resour. Res., 55, 10918– 10934, https://doi.org/10.1029/2019WR025222, 2019.
- Molteni, C. M.: The Effects of COVID-19 Pandemic on Spanish Protected Areas: the Case of Picos de Europa National Park, Rev. Kawsaypacha: Sociedad y Medio Ambiente, 10, 1–21, https://doi.org/10.18800/kawsaypacha.202202.002, 2022.
- Morton, A.: Heavy minerals in provenance studies, in: Provenance of Arenites, edited by: Zuffa, G., NATO ASI series 148, 249–277, https://doi.org/10.1007/978-94-017-2809-6\_12, 1985.
- Morton, A. and Hallsworth, C.: Identifying provenance-specific features of detrital heavy mineral assemblages in sand-

- stones, Sed. Geol., 90, 241–256, https://doi.org/10.1016/0037-0738(94)90041-8, 1994.
- Morton, A. and Hallsworth, C.: Chapter 7 stability of detrital heavy minerals during burial diagenesis, Dev. Sed., 58, 215–245, https://doi.org/10.1016/S0070-4571(07)58007-6, 2007.
- Motis, K., Fernández, L. P., and Heredia, N.: Estratigrafía, Sedimentología y significado tectonoestratigráfico de la Formación Calizas de Panda (Moscoviense superior, sector occidental de la Región del Pisuerga-Carrión, Zona Cantábrica, noroeste de España), Stud. Geol. Salmant., 37, 141–180, 2001.
- Navarro, D. and Leyva, F.: Geological map of Sheet no. 31 15-4 (Ribadesella), Geological Map of Spain scale 1:50 000, Second Series (MAGNA), Instituto Geológico y Minero de España (IGME) for consultation (data), https://info.igme.es/cartografiadigital/geologica/Magna50Hoja.aspx?Id=31 (last access: 11 November 2025), 1986.
- Neely, A. B. and DiBiase, R. A.: Sediment controls on the transition from debris flow to fluvial channels in steep mountain ranges, Earth Surf. Proc. Landf., 48, 1342–1361, https://doi.org/10.1002/esp.5553, 2023.
- Nguyen, V. N., Nguyen, Q. M., Thao, D. T. H., and Huang, S.-C.: An Investigation of Dissimilar Welding Aluminium Alloys to Stainless Steel by Tungsten Inert Gas (TIG) Welding Process, Mat. Sci. Forum, 904, 19–23, https://doi.org/10.4028/www.scientific.net/MSF.904.19, 2017.
- Oberthür, T., Melcher, F., Goldmann, S., Wotruba, H., Gerdes, A., Dijkstra, A., and Dale, C. W.: Mineralogy and mineral chemistry of detrital heavy minerals from the Rhine River in Germany as evidence to their provenance, sedimentary and depositional history: focus on platinum-group minerals and remarks on cassiterite, columbite-group minerals and uraninit, Int. J. Earth Sci., 105, 637–657, https://doi.org/10.1007/s00531-015-1181-3, 2016.
- Ovín Vega, C.: Inundaciones fluviales en la cuenca del río Sella en junio de 2010 y febrero de 2012. Validación del mapa de peligrosidad por inundaciones en el Bajo Sella, Master's Thesis, University of Oviedo, 83 pp., https://digibuo.uniovi.es/dspace/handle/10651/30789 (last access: 11 November 2025), 2014.
- Palacios, T.: Acritarch assemblages from the Oville and Barrios Formations, northern Spain: A pilot proposal of a middle Cambrian (Series 3) acritarch biozonation in northwestern Gondwana, Rev. Palaeobot. Palynol., 219, 71–105, https://doi.org/10.1016/j.revpalbo.2015.03.008, 2015.
- Perejón, A., Moreno-Eiris, E., Bechstädt, T., Menéndez, S., and Rodríguez-Martínez, M.: New Bilbilian (early Cambrian) archaeocyath-rich thrombolytic microbialite from the Láncara Formation (Cantabrian Mts., northern Spain), J. Iber. Geology, 38, 313–330, https://doi.org/10.5209/rev\_JIGE.2012.v38.n2.40461, 2012.
- Pérez-Cejuela, V. S.: Las mineralizaciones de fluorita del ne de asturias: Caracterización y evolución del proceso hidrotermal, Doctoral dissertation, PhD Thesis, Universidsad Complutense de Madrid, 196 pp., https://docta.ucm.es/entities/ publication/93381b8d-a5eb-4fbb-9689-95b95b55e731 (last access: 11 November 2025), 2009.
- Pettijohn, F. J.: Persistence of Heavy Minerals and Geologic Age, J. Geol., 49, 610–625, https://doi.org/10.1086/624992, 1941.
- Pitlik, J., Recking, A., Liebault, F., Misset, C., Piton, G., and Vazquez-Tarrio, D.: Sediment Production in French

- Alpine Rivers, Water Resour. Res., 57, e2021WR030470, https://doi.org/10.1029/2021WR030470, 2021.
- Poldervaart, A.: Zircon in rocks. 2. Igneous rocks, Am. J. Sci., 254, 521–554, https://doi.org/10.2475/ajs.254.9.521, 1956.
- Ramachandra, S. S., Wiehe, S., Hyland, M. M., Chen, X. D., and Bansal, B.: A preliminary study of the effect of surface coating on the initial deposition mechanisms of dairy fouling, in: ECI Symposium Series, RP2, edited by: Müller-Steinhagen, H., Malayeri, M. R., and Watkinson, A. P., Proceedings of the 6th International Conference on Heat Exchanger Fouling and Cleaning Challenges and Opportunities, 88–96, https://dc.engconfintl.org/heatexchanger2005/15 (last access: 11 November 2025), 2005.
- Rittenhouse, G.: Transportation and deposition of heavy minerals, Bull. Geol. Soc. Am., 54, 1725–1780, https://doi.org/10.1130/GSAB-54-1725, 1943.
- Rodríguez-Fernández, L. R., López Olmedo, F., Oliveira, J. T., Medialdea, T., Terrinha, P., Matas, J., Martín-Serrano, A., Martín-Parra, L. M., Rubio, F., Marín, C., Montes, M., and Nozal, F.: Geological Map of Spain and Portugal, Scale 1:1000000, Rodríguez Fernández, L. R. and Oliveira, J. T., IGME-LNEG, Madrid, ISBN 978-84-7840-949-5, 2015.
- Rösler, H. J.: Lehrbuch der Mineralogie, VEB Deutscher Verlag für Grundstoffindustrie, 4th edn., 844 pp., 1988.
- Ruiz Fernández, J. and Poblete Piedrabuena, M. Á.: Las terrazas fluviales del río Cares: aportaciones sedimentológicas y cronológicas (Picos de Europa, Asturias), Est. Geogr., LXXII, 173–202, https://doi.org/10.3989/estgeogr.201108, 2011.
- Sanz-López, J. and Blanco-Ferrera, S.: La Formación Ermita y su significado en la cordillera Varisca, Geogaceta, 74, 11–14, https://doi.org/10.55407/geogaceta98206, 2023.
- Scholz, T. and Gärtner, A.: Initial results from SEM-EDX and LA-ICP-MS chemical characterisation of barium titanate glass microspheres, Forensic Chem., 38, 100569, https://doi.org/10.1016/j.forc.2024.100569, 2024.
- Stevens, A. W., Ruggiero, P., Parker, K. A., Vitosek, S., Gelfenbaum, G., and Kaminsky, G. M.: Climate controls on longshore sediment transport and coastal morphology adjacent to engineered inlets, Coast. Eng., 194, 104617, https://doi.org/10.1016/j.coastaleng.2024.104617, 2024.
- Suárez, O., Cuesta, A., Gallastegui, G., and Corretgé, L. G.: Mineralogía y petrología de las rocas plutónicas de Infiesto (Zona Cantábrica, N. de España), Trab. Geol., 19, 123–153, 1993.
- Suárez Rodriguez, A.: Estructura del área de Villaviciosa-Libardón (Asturias, Cordillera Cantábrica), Trab. Geol. Univ. Oviedo, 17, 87–98, 1988.
- Sun, X., Kuiper, K. F., Tian, Y., Li, C., Gemignani, L., Zhang, Z., and Wijbrans, J. R.: Impact of hydraulic sorting and weathering on mica provenance studies: An example from the Yangtze River, Chem. Geol., 532, 119359, https://doi.org/10.1016/j.chemgeo.2019.119359, 2020.

- Symons, D. T. A., Kawasaki, K., Tornos, F., Velasco, F., and Rosales, I.: Temporal constraints on genesis of the Caravia-Berbes fluorite deposits of Asturias, Spain, from paleomagnetism, Ore Geol. Rev., 80, 754–766, https://doi.org/10.1016/j.oregeorev.2016.08.020, 2017.
- Syvitski, J. P. M. and Milliman, J. D.: Geology, Geography, and Humans Battle for Dominance over the Delivery of Fluvial Sediment to the Coastal Ocean, J. Geol., 115, 1–19, https://doi.org/10.1086/509246, 2007.
- Valenzuela Fernández, M. F. C.: Estratigrafía, sedimentología y paleogeografía del Jurásico de Asturias. Doctoral dissertation, PhD Thesis, Universidsad de Oviedo, 748 pp., https://digibuo.uniovi.es/dspace/handle/10651/15698 (last access: 11 November 2025), 1989
- van Andel, T. H.: Provenance, transport and deposition of Rhine sediments, Veenman, 129 pp., https://hdl.handle.net/11370/8533ead4-1ad0-4a99-a61e-ff012ce7c63d (last access: 11 November 2025), 1950.
- van Loevezijn, G. B. S. and Raven, J. G. M.: The Upper Devonian of the river Sil area: a stratigraphic correlation between León and Asturias, northern Spain, Bol. Geol. Min., 132, 325–354, https://doi.org/10.21701/bolgeomin.132.3.005, 2021.
- Vermeesch, P., Resentini, A., and Garzanti, E.: An R package for statistical provenance analysis, Sed. Geol., 336, 14–25, https://doi.org/10.1016/j.sedgeo.2016.01.009, 2016.
- Weil, A., Gutiérrez-Alonso, G., and Conan, J.: New time constraints on lithospheric-scale oroclinal bending of the Ibero-Armorican Arc: a palaeomagnetic study of earliest Permian rocks from Iberia, J. Geol. Soc., 167, 127–143, https://doi.org/10.1144/0016-76492009-002, 2010.
- Yang, S., Wang, Z., Guo, Y., Li, C., and Cai, J.: Heavy mineral compositions of the Changjiang (Yangtze River) sediments and their provenance-tracing implication, J. Asian Earth Sci., 35, 56–65, https://doi.org/10.1016/j.jseaes.2008.12.002, 2009.
- Yang, T., Liu, Q., Li, H., Zeng, Q., and Chan, L.: Anthropogenic magnetic particles and heavy metals in the road dust: Magnetic identification and its implications, Atm. Envir., 44, 1175–1185, https://doi.org/10.1016/j.atmosenv.2009.12.028, 2010.
- Zamarreño, I. and Julivert, M.: Estratigrafía del Cámbrico del oriente de Asturias y estudio petrográfico de las facies carbonatadas, Trab. Geol., 1, 135–165, https://reunido.uniovi.es/index.php/TDG/article/view/2660 (last access: 11 November 2025), 1967.
- Zhang, C., Qiao, Q., Appel, E., and Huang, B.: Discriminating sources of anthropogenic heavy metals in urban street dusts using magnetic and chemical methods, J. Geochem. Explor., 119–120, 60–75, https://doi.org/10.1016/j.gexplo.2012.06.014, 2012.
- Zoleikhaei, Y., Frei, D., Morton, A., and Zamanzadeh, S. M.: Roundness of heavy minerals (zircon and apatite) as a provenance tool for unraveling recycling: A case study from the Sefidrud and Sarbaz rivers in N and SE Iran, Sed. Geol., 342, 106–117, https://doi.org/10.1016/j.sedgeo.2016.06.016, 2016.